

Transmission mode impacts parasite spread in spatially structured environments

Franziska A. Brenninger^{1*} and Xiang-Yi Li Richter^{1,2}

^{1*}Institute of Ecology and Evolution, University of Bern, Baltzerstrasse
6 , 3012, Bern, Switzerland.

²Department of Biology, University of Konstanz, Universitätsstraße 10,
78464, Konstanz, Germany.

*Corresponding author(s). E-mail(s): f.brenninger.evobio@outlook.com;

Keywords: transmission mode, parasite, vertical transmission, horizontal
transmission, mixed-mode transmission, dispersal, spatial structure, infection spread

Author Contributions Conceptualization: F.A.B. and X.Y.L.R.; Creation of the
model: F.A.B. and X.Y.L.R.; Analyses of results: F.A.B.; writing of first draft:
F.A.B.; revision and editing of the manuscript: F.A.B. and X.Y.L.R.

Data accessibility statement Data and code to reproduce results and figures of
the manuscript can be made available upon request and will be made openly available
after publication.

1 **Abstract**

2 The spread of parasites and pathogens is shaped by their transmission to new hosts
3 and often inherently linked to the spatial structure of host populations. Transmission
4 modes are typically classified as either horizontal — between individuals — or ver-
5 tical, from parent to offspring. While some parasites rely exclusively on one mode,
6 many use both. We investigate how transmission mode impacts the spread of a par-
7 asite in different spatially structured metapopulations with variable habitat size and
8 host dispersal propensity depending on infection status. We find that patch size dis-
9 parities together with infection dependent dispersal result in local infection prevalence
10 that deviates from single patch expectations, whereby the nature of this deviation
11 differs depending on transmission mode. This work shows how parasite transmission
12 mode alters infection spread through spatially structured environments and highlights
13 that transmission modes can have distinct impacts on the evolution of host-parasite
14 dynamics with potential consequences for disease management.

1 Introduction

Parasite transmission is an essential part of host-parasite dynamics, as parasites balance the exploitation of the current host with transmission to the next to achieve optimal lifetime fitness (Anderson and May 1982; Ewald 1983; Massad 1987). Similar to virulence, transmission of a parasite is the result of combining multiple parasite and host traits, such as the parasite's ability to infect and establish in a new host and the host's immune defense (Antonovics et al. 2017). In general, transmission mode is broadly categorized as either vertical, meaning the parasite transmits from parent to offspring, or horizontal, where parasites transmit from one host to the next, independent of relatedness. While some parasites predominantly use one transmission mode (e.g., vertically transmitted endosymbionts in arthropods (Hurst and Frost 2015); horizontal transmission of measles (Getahun et al. 2017) or rabies virus (Hankins and Rosekrans 2004)), others spread through a mix of modes (see (Ebert 2013) for a review), and for many, the full range of transmission pathways remain yet to be identified (Antonovics 2017).

The overarching categories of transmission mode can be further subdivided to specify the nature of parasite transmission in more detail (Antonovics et al. 2017). For instance, vector-borne, airborne, or environmentally transmitted diseases all transmit horizontally, but follow different dynamics when transmitting to a new host. Horizontal transmission of pathogens that spread via vector species, like Malaria or Dengue virus (Meibalan and Marti 2017; Cattarino et al. 2020), or parasites that are passed through sexual contact between hosts, such as Chlamydia or Gonorrhea (Da Ros and da Silva Schmitt 2008), are often modeled as frequency-dependent. The underlying assumption is that each infected individual makes a constant number of potentially infectious contacts per unit time, for example, the number of sexual contacts in a population or the biting rate of a mosquito. Then, the chance of becoming infected primarily depends on the frequency of infected individuals in a population. The spread of other horizontally transmitted parasites is better described by density-dependent (mass-action) transmission. This applies whenever contact rates between

45 individuals change with host density, as is the case in airborne diseases, when released
46 droplets or aerosols can infect more hosts the more individuals are present (McCallum
47 et al. 2001; Begon et al. 2002; Thrall et al. 1993).

48
49 Furthermore, the transmission of a parasite is inherently linked with spatial struc-
50 ture, as host populations tend to be distributed across different habitats and parasites
51 need to move directly or indirectly to encounter susceptible hosts. Incorporating
52 space into host-parasite dynamics yields key insights into epidemiology and parasite
53 ecology (Riley 2007; Guégan et al. 2005). For instance, metapopulation models have
54 shown that connectivity between patches shapes local oscillatory infection dynamics
55 (Xia et al. 2004). Similarly, specific levels of dispersal in a metapopulation can main-
56 tain infections that would not persist in a single well-mixed population (Hagenaars
57 et al. 2004) or limit infection to isolated subpopulations (Post et al. 1983). The
58 most tractable metapopulation framework is a two-patch model, in which dispersal
59 connects patches that may differ in size (as in mainland–island systems). Two-patch
60 models have been applied widely to examine how various ecological processes play out
61 in a spatially structured environment (Grumbach et al. 2023; Szilágyi and Meszéna
62 2009; Cressman and Křivan 2013; Acevedo et al. 2015). Extending these two patch
63 models to randomly generated networks of multiple interconnected patches allows
64 for increased realism while maintaining interpretability of the core dynamics. For
65 instance, randomly generated networks have been used to estimate epidemiological
66 disease waves (Lang et al. 2018; Lloyd and Jansen 2004) and population persistence
67 in fragmented landscapes (Grilli et al. 2015), which clarify the building blocks for
68 metapopulation models that add more biological complications, such as locally vari-
69 able infection rates (Acevedo et al. 2015) or stage specific extinction risks (Sutherland
70 et al. 2014).

71
72 It is well established that transmission mode is a key determinant of parasite
73 spread and persistence within a single patch (Lipsitch et al. 1995, 1996). However,
74 existing spatially structured models typically focus on a single transmission mode

75 inspired by a host–parasite pairing of interest (Lloyd and Sattenspiel 2009; Fulford
76 et al. 2002; Hickson et al. 2012; Gaff and Gross 2007; Zeng et al. 2023), which limits
77 general insights across systems. The few cases examining parasites with multiple
78 transmission modes, usually involving at most two, demonstrate that transmission
79 can strongly shape spatial patterns of infection (Shaw et al. 2019; Fulford et al. 2002;
80 Berngruber et al. 2015; Ryder et al. 2007).
81 Thus, despite substantial progress in spatial epidemiology and parasite ecology, a
82 priori expectations of whether and to what extent different transmission modes shape
83 parasite spread across space remains unexplored.

84

85 Here, we adopt a systematic approach to examine how commonly consid-
86 ered parasite transmission modes — frequency-dependent horizontal transmission,
87 density-dependent horizontal transmission, vertical transmission, and corresponding
88 mixed-mode transmissions — interact with spatial structure to shape parasite spread
89 and prevalence. Extending classical SIS (susceptible-infected-susceptible) frameworks,
90 we develop spatially explicit UIU (uninfected–infected–uninfected) models. Here, we
91 adapt the terminology to account for the fact that, under exclusive vertical trans-
92 mission, uninfected individuals are per definition never ‘susceptible’. To establish
93 baseline expectations for how transmission mode, host dispersal and spatial structure
94 influence infection spread, we analyze parasite dynamics across one-patch, two-patch,
95 and randomly generated network scenarios. By providing a unified framework that
96 isolates the effects of transmission mode under comparable conditions, this study aims
97 to advance fundamental understanding in spatial epidemiology and inform future
98 theoretical and empirical work on parasite invasion and disease dynamics. We also
99 highlighting the importance of transmission mode for host-parasite dynamics and its
100 potential for evolutionary adaptation.

101

102 2 Material and methods

103 To investigate how transmission mode of a parasite influences infection dynam-
104 ics, we adapt several UIU models to compare a total of five different transmission
105 modes: (1) frequency-dependent horizontal transmission (FD), (2) density-dependent
106 horizontal transmission (DD), (3) vertical transmission (V), (4) mixed-mode trans-
107 mission with frequency-dependent horizontal and vertical transmission (FD+V) and
108 (5) mixed-mode transmission with density-dependent horizontal and vertical trans-
109 mission (DD+V) (Figure 1). In the following, we derive the infection dynamics for a
110 parasite using mixed-mode transmission, as this includes all components of the indi-
111 vidual transmission modes. The detailed derivations for each individual transmission
112 mode are provided in Supplementary Information S1. We first detail the dynamics
113 within a single isolated patch, before adding spatial structure to our model later.

114 2.1 Single patch dynamics

115 We assume a well-mixed, asexually reproducing population of uninfected and infected
116 individuals, denoted by U and I , respectively. Total population size N is calculated
117 as $N = U + I$. We can describe the infection dynamics in a population infected with
118 a parasite that can transmit both horizontally and vertically as

$$\begin{aligned}\frac{dU}{dt} &= \alpha_U U + \alpha_I (1 - \beta_v) I + \mu I - \Omega - d_U U - \theta N U, \\ \frac{dI}{dt} &= \alpha_I \beta_v I + \Omega - \mu I - d_I I - \theta N I.\end{aligned}\tag{1}$$

119 Here, α is the per capita growth rate and d the baseline mortality for uninfected and
120 infected individuals, as indicated by the subscript U and I , respectively. We assume
121 that both fertility and mortality can differ with infection state, as infected individuals
122 may experience higher mortality and reduced fertility compared to healthy con-
123 specific. The population is subject to density-dependent mortality, where increased
124 crowding in the environment results in higher mortality. This effect is scaled by the
125 parameter θ , modulating the strength of density-dependent mortality.

126 Individuals can inherit the parasite (vertical transmission) or get infected during
127 their life (horizontal transmission). Vertical transmission efficiency is denoted by β_v ,

128 representing the proportion of offspring that inherit the parasite from an infected par-
 129 ent. The remaining proportion $1 - \beta_v$ consists of offspring that did not inherit the
 130 parasite due to transmission failure and is instead added to the number of uninfected
 131 individuals in the population. Horizontal transmission is captured by infection rate Ω .
 132 In cases where horizontal transmission is frequency dependent, Ω takes the form of
 133 $c\beta_h \frac{I}{N}U$, where c is the encounter rate between individuals. The probability of encoun-
 134 tering an infected individual is given by the frequency of infected individuals in the
 135 population, $\frac{I}{N}$, and upon contact, horizontal transmission of the parasite occurs with
 136 horizontal transmission efficiency β_h . When horizontal transmission is density depen-
 137 dent, Ω takes the form of $c\beta_h IU$. In this case, the transmission of infection increases
 138 as population density grows (density-dependent or mass-action infection). Thus, the
 139 rate of new infections is proportional to the number of infected and uninfected individ-
 140 uals in the population IU and scaled by the contact rate and transmission efficiency
 141 of the parasite $c\beta_h$. Infected individuals can recover and lose the infection at rate μ .
 142 See Figure 1 for a flow diagram corresponding to equations 1 and Table 1 for a list of
 143 all symbols.

144 2.2 Dynamics with spatial structure

145 To determine how infection dynamics can differ in a spatially structured system, we
 146 consider a set of distinct habitats — also referred to as patches — connected by the
 147 dispersal of individuals between them. The dynamics of such a system are then the
 148 combined result of local infection spread and dispersal between patches, which we
 149 describe following jansen2000local with

$$\hat{x}_j = f(x_j) + \sum_{i=1}^n s_{ij} \mathbf{M} x_i. \quad (2)$$

150 Here, x_j denotes a vector containing the densities of the different types of individu-
 151 als (U, I) within patch j , with $f(x_j)$ accounting for the local dynamics. Local dynamics
 152 are defined depending on the transmission mode (see equations 1, S1, S4, S8, S11, S14).
 153 The diagonal migration matrix \mathbf{M} denotes dispersal propensity for the different types

154 of individuals, while the connections between the patches is described by the connec-
155 tivity matrix \mathbf{S} . Hereby, we assume that infected and uninfected individuals can reach
156 the same habitats, but the proportion of individuals that disperse can differ depending
157 on infection state. Infected individuals, for example, may become more or less likely to
158 move to a new patch compared to uninfected con-specifics (Bradley and Altizer 2005;
159 Debeffe et al. 2014; Brophy and Luong 2022). Thus, we define two different dispersal
160 propensities m_U and m_I , referring to uninfected and infected individuals, respectively.
161 Individuals cannot get infected or recover during dispersal, meaning that infection
162 status can only change within a patch.

163 **2.2.1 Mainland-island model**

164 First, we consider a case with two habitats of different sizes that are connected by
165 dispersing individuals. The size difference between the two habitats is determined
166 by the patch specific density-dependent mortality θ_i, θ_j . A larger density-dependent
167 mortality θ , corresponds to a smaller habitat, where individual mortality increases at
168 comparatively lower levels of crowding. Note that this form of population size regu-
169 lation does not impose a strict carrying capacity. See Supplementary Information S2
170 and equations therein for concrete examples of implementation of two-patch dynamics
171 for each transmission mode.

172 **2.2.2 Randomly generated networks**

173 We next extend our analysis by simulating the effects of different transmission modes
174 within more complex spatial structures by considering a network of multiple patches
175 generated by a random geometric graph. To generate the network, we assign a location
176 to each patch, by randomly picking x - and y - coordinates between 0 and 1 following
177 a uniform distribution. Patch connections are determined by the network connect-
178 edness parameter a , defining the maximum distances within which patches remain
179 connected. If the distance between patch i and j is smaller or equal to a , the two
180 habitats are connected, otherwise habitats are too distant from each other to allow
181 successful dispersal.

Table 1 Symbols and meanings.

| Symbol | Meaning |
|-------------------|--|
| U | Number of uninfected individuals in the population |
| I | Number of infected individuals in the population |
| N | Total population size calculated by $N = U + I$ |
| α_U | Per capita growth rate of uninfected individuals |
| α_I | Per capita growth rate of infected individuals |
| β_h | Horizontal transmission efficiency |
| β_v | Vertical transmission efficiency |
| c | Contact rate |
| d_U | Baseline mortality of uninfected individuals |
| d_I | Baseline mortality of infected individuals |
| θ | Strength of population density regulation |
| μ | Recovery rate from infection |
| Subscripts i, j | Subscripts i and j refer to two different patches |
| x_j | Vector containing the densities of the different types of individuals (U, I) in patch j |
| M | Migration matrix containing dispersal probabilities |
| m_U, m_I | Dispersal probability for uninfected and infected individuals |
| S | Connectivity matrix describing spatial structure of the different patches |
| $s_{i,j}$ | Elements of the connectivity matrix describing the connection from patch i to j |
| a | Network connectedness in a geometric network graph describing the maximum distance at which two patches can be connected |

182 3 Results

183 Quantitative comparisons between the different transmission modes are inherently
184 challenging, as each mode is characterized with somewhat distinct parameters. Fur-
185 ther, the effect of a parameter can scale differently within each mode. At low values
186 of $c < 0.1$, for example, frequency-dependent transmission can fail to produce sus-
187 tained infection spread, whereas the same values may suffice when transmission is
188 density-dependent. To account for such disparities and avoid instant fixation of, for
189 example, density-dependent infection, we chose different c values for the two horizon-
190 tal transmission modes in the results below. While this precludes direct quantitative

191 comparison between the different transmission modes, we here focus on a qualitative
192 comparison with the aim to understand the interaction between infection dynamics of
193 parasites utilizing different transmission modes across different spatial structures.

194 3.1 Single patch dynamics

195 Within a single patch, distinct infection dynamics arise from the different transmission
196 modes. The main difference between the two horizontal transmission modes is whether
197 transmission can be amplified by higher population density (density-dependence) or
198 higher infection frequency (frequency-dependence). A parasite that is transmitted
199 solely horizontally in a frequency-dependent manner, would reduce its own transmis-
200 sion when conferring a fecundity benefit to infected hosts, because infected individuals
201 only produce uninfected offspring. With increased birth of uninfected offspring the
202 infection frequency in the population lowers, which results in less infection transmission
203 (following $c\beta_h \frac{I}{N}U$) (Figure 2a). In contrast, higher host fecundity with a density-
204 dependent horizontally transmitting parasite can speed up transmission as individuals
205 accumulate in the patch. Regardless, the parasite will reach the same equilibrium
206 frequency independent of host fecundity, as long as maximum patch population size
207 remains stable (Figure 2b). While horizontally transmitted parasites can spread even
208 when infection imposes a fecundity costs on the host (e.g., $\alpha_I < 1$, when $\alpha_U = 1$),
209 provided that transmission efficiency (β_h) and contact rate (c) are sufficiently high —
210 vertically transmitted parasites require high transmission efficiency β_v and/or a fecun-
211 dity advantage in infected hosts (e.g., $\alpha_I > 1$, when $\alpha_U = 1$) to spread in a population
212 (Figure 2c).

213 These insights extend to mixed-mode transmission (Figure 2d,e). When mixed-
214 mode includes frequency-dependent horizontal transmission (FD+V), the benefits that
215 increased fecundity in infected individuals brings to vertical transmission weigh against
216 the reduction in transmission for FD horizontal transmission, such that the equilib-
217 rium infection prevalence varies depending on which transmission mode is used more
218 (Figure 2d). When transmission is density-dependent horizontal and vertical (DD+V),
219 a fecundity boost in infected hosts ($\alpha_I > \alpha_U$) generally increases the equilibrium

220 infection frequency in a patch (Figure 2e). In the mixed-mode transmission cases, the
221 proportion of horizontally transmitted infections initially rises with population size
222 under density-dependent transmission but remains stable under frequency-dependent
223 transmission. In both cases, the proportion of new infections arising from horizontal
224 or vertical transmission changes with increasing infection prevalence in the population
225 (Figure S8), so that the proportion of infection by horizontal transmission declines as
226 the parasite becomes widespread in the population and most new infections are gained
227 via the vertical transmission pathway.

228 **3.2 Spatial structure**

229 **3.2.1 Mainland-island model**

230 In the mainland-island scenario, when patches are of equal size, infection prevalence
231 converges on the same equilibrium in both habitats matching the single-patch case,
232 because the number of individuals leaving a patch matches the number of individuals
233 arriving irrespective of the dispersal propensity of the individuals (Figure S9a-e).
234 When the two patches differ in size, the number of dispersers arriving no longer equals
235 the number of dispersers leaving. Differences in dispersal propensity between infected
236 and uninfected individuals can then alter the infection prevalence in both patches.
237 Generally, the type of individual (infected or uninfected) that disperses more tends
238 to accumulate in higher numbers in the smaller patch, shifting the local prevalence
239 toward the more dispersive type. In the larger patch, more of the dispersive individu-
240 als leave the patch than enter from the smaller patch, which biases the composition
241 there toward individuals that are more likely to stay. For example, when infected
242 individuals disperse more readily than uninfected ones, infection prevalence tends
243 to be higher in the smaller patch, while the infection prevalence in the larger patch
244 is comparatively reduced. When dispersal rates do not vary with infection status,
245 the system converges on the same infection prevalence in both patches (Figure 3a,d;
246 white diagonal line). Similarly, there are no infection prevalence differences between
247 the patches, when there are only infected individuals in both patches.

248

249 Deviations from this pattern occur under specific parameter combinations for
250 some of the transmission modes. In the case of density-dependent horizontal trans-
251 mission, higher population density of the larger patch leads to increased transmission
252 compared to the smaller patch. This amplified transmission rate in the larger patch
253 can partially offset net migration losses (individuals arriving; individuals leaving) of
254 infected individuals, so that under some parameter combinations, the larger patch
255 may still have a higher infection prevalence than the smaller patch, even when infected
256 individuals disperse more than uninfected ones (Figure 3b,e; note the shift in the
257 white diagonal line compared to a and d). As the disparity in patch size increases, this
258 effect diminishes, because increasingly negative net migration continuously reduces
259 population density in the larger patch, consequently lowering density-dependent
260 transmission (Figure 3; shift of the white line from b to e).

261

262 In the case of vertical transmission, (infected) individuals arriving in a patch do
263 not impact transmission in the same way as they do under frequency- or density-
264 dependent horizontal transmission. Instead, absolute numbers of immigrants and
265 emigrants play a more direct role in determining infection prevalence, leading to
266 noticeably distinct dynamics when patch size difference increases (Figure 3c,f).
267 Importantly, even if individuals of a certain infection status are more likely to dis-
268 perse, this does not necessarily result in a higher number of dispersers in absolute
269 terms. For instance, if infected individuals have higher dispersal propensity, the larger
270 patch will contain fewer of them due to sustained negative net migration (i.e. the
271 number of infected individuals leaving exceeds the number arriving). In contrast, the
272 dispersal propensity of uninfected individuals is smaller, corresponding to a smaller
273 net migrational loss of uninfected individuals in the larger patch. As a result, the
274 larger habitat equilibrates at low infection prevalence. Then, even if the proportion
275 of infected dispersers is higher than the proportion of uninfected ones, the absolute
276 number of infected dispersers arriving in a patch can fall below the number of unin-
277 fected dispersers arriving, resulting in low infection prevalence in the smaller patch
278 (Figure 4a-e). However, when uninfected individuals are very philopatric and the

279 proportion of uninfected dispersers is so small that the absolute number of uninfected
280 dispersers remains lower than that of infected dispersers, the smaller patch can
281 reach high infection prevalence even when the larger patch contains predominantly
282 uninfected individuals (Figure 3d-h). The same reasoning can explain the patterns
283 emerging when uninfected individuals tend to disperse more than infected ones
284 (Figure 4d,e).

285

286 **3.2.2 Randomly generated network**

287 We extended our analysis to more complex spatial structures by considering dispersal
288 in habitat networks modeled by random geometric graphs. Network connectedness
289 at a given value of a may lead to different numbers of connected patches across
290 replicates, depending on the random spatial patch distribution (Figure 5a,b). As
291 network connectedness a expands — and each patch becomes linked to more neigh-
292 bors — the average infection prevalence in the network increases. The structural
293 heterogeneity between the replicates results in variation in global infection prevalence
294 at intermediate levels of connectedness (Figure 5c-f). Global infection prevalence also
295 varies between transmission modes, and similar to the single and two-patch models,
296 mixed-mode transmission produces the highest global infection prevalence compared
297 to vertical or horizontal transmission alone (Figure 5c-f). Infection dynamics of para-
298 sites using different transmission modes also diverge, when comparing two networks
299 with the same number of patches and maximum patch size but contrasting patch
300 size distributions: one with patches of two different sizes (maximum and 1/5th of the
301 maximum, Figure 5a,c,e) and one where the size distribution of the patches gradually
302 decreases to 1/10th of the maximum patch size (Figure 5b,d,f). Vertically transmit-
303 ted parasites are most notably impacted by varying dispersal propensity and patch
304 size differences, as increased dispersal of uninfected hosts amplifies global infection
305 prevalence, while greater variation in patch size combined with higher dispersal of
306 infected hosts reduces the resulting global infection prevalence (Figure 5c-f, Supple-
307 mentary Figures S10, S11, S12). In the network with gradually decreasing patch sizes,

308 infection prevalence for density-dependent horizontally transmitted parasites is lower
309 compared to the network composed of two different patch sizes, because the smaller
310 sized patches and therefore reduced local population density constrains transmission
311 and subsequently lowers prevalence (Figure 5c,e versus d,f). Similarly, network com-
312 position and dispersal propensity affect the speed with which parasites reach global
313 infection equilibrium in a randomly generated network and their influence of these
314 factors on the time until global equilibrium differ qualitatively between transmission
315 modes (Figure S13).

316

317 4 Discussion

318 Variations to transmission, although central to parasite dynamics, have been less of a
319 focal point in epidemiological studies than other parts of host parasite interactions,
320 such as virulence. Along with recent work increasingly considering multiple and more
321 complex transmission modes, our findings highlight that transmission mode substan-
322 tially alters parasite spread through space when coupled with varying spatial structure
323 and infection status dependent dispersal. Depending on horizontal transmission mode
324 the number of horizontal transmission events in a patch can change with infection
325 frequency or host density - both factors that are influenced by status dependent
326 dispersal propensity. While vertical transmission is naturally linked with the rate of
327 host reproduction. These features have consequences for infection dynamics in space,
328 for example, patch size variation will impact the global equilibrium frequency of
329 density-dependent horizontally transmitted parasites and higher dispersal of infected
330 individuals slows the spread of parasites using frequency-dependent horizontal or
331 vertical transmission in a patch. While horizontally transmitted parasites can com-
332 pensate net migratory losses to some extent by enhanced transmission when dispersal
333 leads to locally increased population density or infection frequency, vertically trans-
334 mitted parasites rely more strictly on dispersal numbers to establish in new habitats.

335

336 Our findings for the single-patch infection dynamics are consistent with those of
337 (Lipsitch et al. 1995), who examined parasite dynamics when using density-dependent
338 horizontal, vertical or mixed-mode transmission, in a well-mixed population. We add
339 to the previous results by incorporating frequency-dependent horizontal transmission
340 and adding spatial structure. Vertically transmitted parasites require sufficiently high
341 host fecundity and transmission efficiency to increase in frequency (Ewald 1987; Fine
342 1984; Lipsitch et al. 1995), making infected host reproduction a non-negligible factor
343 in the dynamics of vertical and mixed-mode transmission. While some parasites can
344 completely castrate hosts upon infection (Baudoin 1975; Lafferty and Kuris 2009)
345 many do not, and an increasing body of evidence suggests that boosting reproductive
346 effort as a response to infection can also act as a form of tolerance to offset the ele-
347 vated mortality caused by parasite virulence (Roy and Kirchner 2000; Råberg et al.
348 2007; Brenninger et al. 2025).

349
350 Host-parasite models often consider a horizontally transmitting parasite (Lloyd
351 and Sattenspiel 2009; Hickson et al. 2012; Best et al. 2017; Shaw et al. 2019), but
352 many pathogens can transmit through multiple modes or routes (Antonis et al. 2013;
353 Ebert 2013; Pagán et al. 2014; García-Ordóñez and Pagán 2024). Adding vertical
354 transmission to a horizontal transmission mode (FD+V and DD+V) outperforms the
355 models of each individual transmission mode in terms of increasing infection preva-
356 lence and reducing time until global equilibrium, even when parasitic infection comes
357 with a fecundity cost. When a parasite transmits through more than one mode, feed-
358 back can arise between the different transmission modes and population composition.
359 Within a single patch, the relative contribution of the different transmission modes
360 shifts as infection prevalence increases: in both mixed-mode scenarios, the proportion
361 of new infections via horizontal transmission declines as susceptible hosts become
362 scarce, and vertical transmission increasingly contributes to new infections (Lipsitch
363 et al. 1995, 1996). Similar dynamics have been reported for mixed-mode transmission
364 in a lattice-structured population model, where a virulent strain initially transmits
365 predominantly through horizontal transmission, but as susceptible hosts become

366 scarce, the strain is mainly transmitted vertically (Berngruber et al. 2015). While we
367 focused on our analyses on combinations of different vertical and horizontal trans-
368 mission modes, transmitting via more than one horizontal transmission mode, for
369 example, via sexual and airborne pathways, can also strongly affect parasite dynamics
370 in spatially structured populations. For instance, equipping a predominantly density-
371 dependent transmitting parasite with low levels of frequency-dependent transmission
372 has been shown to enhance infection persistence in spatially structured environments,
373 while adding minor density-dependent transmission to a frequency-dependent para-
374 site can increase the chances of parasite-driven extinction (Ryder et al. 2007).

375

376 Dispersal propensity and patch sizes are critical determinants of infection preva-
377 lence in spatially structured populations. Consistent with our findings, a two-patch
378 metapopulation model of horizontal tuberculosis transmission in possums shows that
379 differences in patch carrying capacity increase divergence from single-patch predic-
380 tions. Larger disparities also dampen infection oscillations, with the smaller patch
381 often exhibiting higher prevalence (Fulford et al. 2002). Empirical results often find
382 that larger patches or patches with high levels of dispersal towards them maintain
383 higher infection prevalence (Laine and Hanski 2006; van Dijk et al. 2022). Our results
384 illustrate the relative importance of infected and uninfected dispersal propensity to
385 shape these patterns and show conditions where the smaller patches can maintain
386 high infection prevalence. Moreover, the tendency for larger patches to contain higher
387 prevalence in natural populations also reflects a lower local extinction risk, which our
388 model does not explicitly account for.

389

390 We assume an additive benefit for parasites capable of more than one transmis-
391 sion mode in the presented findings. There are empirical examples matching this
392 assumption, for instance, high parasite pressure of the ectoparasite *Ophryocystis elek-*
393 *troscirrho* infecting the American Monarch butterfly (*Danaus plexippus*) enhances
394 transmission via both the horizontal and vertical pathway (De Roode et al. 2009).
395 Contrasting evidence suggests a tradeoff between horizontal and vertical transmission

396 modes in parasites capable of both (Messenger et al. 1999; Turner et al. 1998). In gen-
397 eral, transmission mode is variable and can evolve rapidly (Pagán et al. 2014), or be
398 influenced by a multitude of factors such as competition between different parasites
399 (Harbison et al. 2008; Jones et al. 2011), seasonal variation of host social structures
400 (Smith et al. 2009) or host genotype and environmental conditions (Zilio et al. 2018).
401 Here, our model usefully allows a flexible relationships between transmission modes,
402 where tradeoffs are not explicitly imposed, but can be modeled implicitly, depending
403 on parameter settings.

404

405 Our findings underscore the importance of considering multiple transmission
406 modes when studying disease dynamics and provide a baseline qualitative expectation
407 for the effects of space and dispersal on parasites that utilize different transmission
408 modes. The current model prioritizes generality and is thus less characterized with
409 system-specific biological details, such as the precise transmission routes parasites
410 can employ and their relative importance in a specific natural population (Cottam
411 et al. 2008). Establishing which transmission modes are utilized in nature is essential,
412 as both horizontal and vertical transmission can distinctly shape infection prevalence
413 and eco-evolutionary feedback between host and parasites. At evolutionary scales,
414 host-parasite dynamics are also likely to be sensitive to differences in transmission
415 mode. In particular, since parasites can act as selective forces on host movement
416 patterns (Pérez-Tris and Bensch 2005; Altizer et al. 2011; Mo 1997; Boulinier et al.
417 2016; Shaw et al. 2019), different transmission modes may lead to the evolution of
418 distinct dispersal tendencies under otherwise comparable conditions. An outstanding
419 knowledge gap for future work is thus whether and to what extend different trans-
420 mission modes influence the the evolution of host movement patterns.

421

422 Disentangling effects of transmission mode on host spread provides a baseline for
423 interpreting more complex ecological and evolutionary scenarios and making more
424 informed predictions on the evolution of transmission mode. From an applied perspec-
425 tive, interventions that reduce transmission are often used to manage disease spread

426 and virulence, but their efficacy depends on comprehending the underlying evolution-
427 ary potential of transmission mode and its impact on infection dynamics in spatially
428 structured networks. By clarifying how transmission strategy and spatial dynamics
429 interact, our work provides a conceptual foundation of the factors likely also shaping
430 more complex large scale models and aids to predict disease prevalence dynamics.

431 **Declarations**

432 **Conflict of interest.** The authors have no conflict of interest to declare.

433 **Acknowledgements.** We thank Yuanxiao Gao for insightful discussions and helpful
434 comments on the manuscript draft. Both scientists were funded by the Swiss National
435 Science Foundation (grant number: 211549).

436 **References**

437 Acevedo MA, Prosper O, Lopiano K, Ruktanonchai N, Caughlin TT, Martcheva
438 M, et al. Spatial heterogeneity, host movement and mosquito-borne disease
439 transmission. *PloS one*. 2015;10(6):e0127552.

440 Altizer S, Bartel R, Han BA. Animal migration and infectious disease risk. *science*.
441 2011;331(6015):296–302.

442 Anderson RM, May RM. Coevolution of hosts and parasites. *Parasitology*.
443 1982;85(2):411–426.

444 Antonis A, Kortekaas J, Kant J, Vloet R, Vogel-Brink A, Stockhofe N, et al. Vertical
445 transmission of Rift Valley fever virus without detectable maternal viremia. *Vector-*
446 *borne and zoonotic diseases*. 2013;13(8):601–606.

447 Antonovics J. Transmission dynamics: critical questions and challenges. *Philosophical*
448 *Transactions of the Royal Society B: Biological Sciences*. 2017;372(1719):20160087.

449 Antonovics J, Wilson AJ, Forbes MR, Hauffe HC, Kallio ER, Leggett HC, et al. The
450 evolution of transmission mode. *Philosophical Transactions of the Royal Society B:*

- 451 Biological Sciences. 2017;372(1719):20160083.
- 452 Baudoin M. Host castration as a parasitic strategy. *Evolution*. 1975;p. 335–352.
- 453 Begon M, Bennett M, Bowers RG, French NP, Hazel S, Turner J. A clarification
454 of transmission terms in host-microparasite models: numbers, densities and areas.
455 *Epidemiology & Infection*. 2002;129(1):147–153.
- 456 Berngruber TW, Lion S, Gandon S. Spatial structure, transmission modes and the
457 evolution of viral exploitation strategies. *PLoS pathogens*. 2015;11(4):e1004810.
- 458 Best A, Ashby B, White A, Bowers R, Buckling A, Koskella B, et al. Host–parasite
459 fluctuating selection in the absence of specificity. *Proceedings of the Royal Society*
460 *B: Biological Sciences*. 2017;284(1866).
- 461 Boulinier T, Kada S, Ponchon A, Dupraz M, Dietrich M, Gamble A, et al. Migra-
462 tion, prospecting, dispersal? What host movement matters for infectious agent
463 circulation? *Integrative and comparative biology*. 2016;56(2):330–342.
- 464 Bradley CA, Altizer S. Parasites hinder monarch butterfly flight: implications for
465 disease spread in migratory hosts. *Ecology Letters*. 2005;8(3):290–300.
- 466 Brenninger FA, Kovalov V, Kokko H. Sex-specific immunocompetence: resistance
467 and tolerance can both be futile but not under the same circumstances. *Evolution*
468 *Letters*. 2025;9(2):249–258.
- 469 Brophy T, Luong LT. The influence of infection status and parasitism risk on host
470 dispersal and susceptibility to infection in *Drosophila nigrospiracula*. *Parasitology*.
471 2022;149(5):587–592.
- 472 Cattarino L, Rodriguez-Barraquer I, Imai N, Cummings DA, Ferguson NM. Mapping
473 global variation in dengue transmission intensity. *Science translational medicine*.
474 2020;12(528):eaax4144.

- 475 Cottam EM, Wadsworth J, Shaw AE, Rowlands RJ, Goatley L, Maan S, et al. Trans-
476 mission pathways of foot-and-mouth disease virus in the United Kingdom in 2007.
477 PLoS pathogens. 2008;4(4):e1000050.
- 478 Cressman R, Křivan V. Two-patch population models with adaptive dispersal: the
479 effects of varying dispersal speeds. Journal of mathematical biology. 2013;67(2):329–
480 358.
- 481 Da Ros CT, da Silva Schmitt C. Global epidemiology of sexually transmitted diseases.
482 Asian journal of andrology. 2008;10(1):110–114.
- 483 De Roode JC, Chi J, Rarick RM, Altizer S. Strength in numbers: high parasite bur-
484 dens increase transmission of a protozoan parasite of monarch butterflies (*Danaus*
485 *plexippus*). Oecologia. 2009;161:67–75.
- 486 Debeffe L, Morellet N, Verheyden-Tixier H, Hoste H, Gaillard JM, Cargnelutti B,
487 et al. Parasite abundance contributes to condition-dependent dispersal in a wild
488 population of large herbivore. Oikos. 2014;123(9):1121–1125.
- 489 van Dijk LJ, Ehrlén J, Tack AJ. The relationship between pathogen life-history traits
490 and metapopulation dynamics. New Phytologist. 2022;233(6):2585–2598.
- 491 Ebert D. The epidemiology and evolution of symbionts with mixed-mode transmission.
492 Annual Review of Ecology, Evolution, and Systematics. 2013;44(1):623–643.
- 493 Ewald PW. Host-parasite relations, vectors, and the evolution of disease severity.
494 Annual Review of Ecology and Systematics. 1983;14:465–485.
- 495 Ewald PW. Transmission modes and evolution of the parasitism-mutualism contin-
496 uum. Annals of the New York Academy of Sciences. 1987;503:295–306.
- 497 Fine PE. Vertical transmission of pathogens of invertebrates. In: Pathogens of Inver-
498 tebrates: Application in Biological Control and Transmission Mechanisms. Springer;
499 1984. p. 205–241.

- 500 Fulford GR, Roberts MG, Heesterbeek JA. The metapopulation dynamics of
501 an infectious disease: tuberculosis in possums. *Theoretical population biology*.
502 2002;61(1):15–29.
- 503 Gaff HD, Gross LJ. Modeling tick-borne disease: a metapopulation model. *Bulletin*
504 *of Mathematical Biology*. 2007;69(1):265–288.
- 505 García-Ordóñez L, Pagán I. Vertical and horizontal transmission of plant viruses: two
506 extremes of a continuum? *npj Viruses*. 2024;2(1):18.
- 507 Getahun M, Beyene B, Ademe A, Teshome B, Tefera M, Afework A, et al. Epidemiol-
508 ogy of laboratory confirmed measles virus cases in the southern nations of Ethiopia,
509 2007–2014. *BMC infectious diseases*. 2017;17(1):87.
- 510 Grilli J, Barabás G, Allesina S. Metapopulation persistence in random fragmented
511 landscapes. *PLoS computational biology*. 2015;11(5):e1004251.
- 512 Grumbach C, Reurik FN, Segura J, Franco D, Hilker FM. The effect of dispersal on
513 asymptotic total population size in discrete-and continuous-time two-patch models.
514 *Journal of Mathematical Biology*. 2023;87(4):60.
- 515 Guégan J, Morand S, Poulin R. Are there general laws in parasite community ecology?
516 The emergence of spatial parasitology and epidemiology. *Parasitism and ecosystems*.
517 2005;p. 22–42.
- 518 Hagenaars T, Donnelly C, Ferguson N. Spatial heterogeneity and the persistence of
519 infectious diseases. *Journal of theoretical biology*. 2004;229(3):349–359.
- 520 Hankins DG, Rosekrans JA. Overview, prevention, and treatment of rabies. In: *Mayo*
521 *Clinic Proceedings*, vol. 79 Elsevier; 2004. p. 671–676.
- 522 Harbison CW, Bush SE, Malenke JR, Clayton DH. Comparative transmission
523 dynamics of competing parasite species. *Ecology*. 2008;89(11):3186–3194.

- 524 Hickson RI, Mercer GN, Lokuge KM. A metapopulation model of tuberculosis
525 transmission with a case study from high to low burden areas. *PLoS One*.
526 2012;7(4):e34411.
- 527 Hurst GD, Frost CL. Reproductive parasitism: maternally inherited symbionts in a
528 biparental world. *Cold Spring Harbor perspectives in biology*. 2015;7(5):a017699.
- 529 Jones EO, White A, Boots M. The evolution of host protection by vertically
530 transmitted parasites. *Proceedings of the Royal Society B: Biological Sciences*.
531 2011;278(1707):863–870.
- 532 Lafferty KD, Kuris AM. Parasitic castration: the evolution and ecology of body
533 snatchers. *Trends in parasitology*. 2009;25(12):564–572.
- 534 Laine AL, Hanski I. Large-scale spatial dynamics of a specialist plant pathogen in a
535 fragmented landscape. *Journal of Ecology*. 2006;94(1):217–226.
- 536 Lang JC, De Sterck H, Kaiser JL, Miller JC. Analytic models for SIR disease spread
537 on random spatial networks. *Journal of Complex Networks*. 2018;6(6):948–970.
- 538 Lipsitch M, Nowak MA, Ebert D, May RM. The population dynamics of vertically
539 and horizontally transmitted parasites. *Proceedings of the Royal Society of London*
540 *Series B: Biological Sciences*. 1995;260(1359):321–327.
- 541 Lipsitch M, Siller S, Nowak MA. The evolution of virulence in pathogens with vertical
542 and horizontal transmission. *Evolution*. 1996;50(5):1729–1741.
- 543 Lloyd AL, Jansen VA. Spatiotemporal dynamics of epidemics: synchrony in metapop-
544 ulation models. *Mathematical biosciences*. 2004;188(1-2):1–16.
- 545 Lloyd AL, Sattenspiel L. Spatiotemporal dynamics of measles: synchrony and persis-
546 tence in a disease metapopulation. In: *Spatial ecology*. Chapman and Hall/CRC;
547 2009. p. 277–298.

- 548 Massad E. Transmission rates and the evolution of pathogenicity. *Evolution*. 1987;p.
549 1127–1130.
- 550 McCallum H, Barlow N, Hone J. How should pathogen transmission be modelled?
551 *Trends in ecology & evolution*. 2001;16(6):295–300.
- 552 Meibalan E, Marti M. Biology of malaria transmission. *Cold Spring Harbor*
553 *perspectives in medicine*. 2017;7(3):a025452.
- 554 Messenger SL, Molineux IJ, Bull J. Virulence evolution in a virus obeys a trade
555 off. *Proceedings of the Royal Society of London Series B: Biological Sciences*.
556 1999;266(1417):397–404.
- 557 Mo TA. Seasonal occurrence of *Gyrodactylus derjavini* (Monogenea) on brown trout,
558 *Salmo trutta*, and Atlantic salmon, *S. salar*, in the Sandvikselva river, Norway. *The*
559 *Journal of parasitology*. 1997;p. 1025–1029.
- 560 Pagán I, Montes N, Milgroom MG, García-Arenal F. Vertical transmission selects for
561 reduced virulence in a plant virus and for increased resistance in the host. *PLoS*
562 *Pathogens*. 2014;10(7):e1004293.
- 563 Pérez-Tris J, Bensch S. Dispersal increases local transmission of avian malarial
564 parasites. *Ecology Letters*. 2005;8(8):838–845.
- 565 Post W, DeAngelis D, Travis C. Endemic disease in environments with spatially
566 heterogeneous host populations. *Mathematical Biosciences*. 1983;63(2):289–302.
- 567 Riley S. Large-scale spatial-transmission models of infectious disease. *Science*.
568 2007;316(5829):1298–1301.
- 569 Roy B, Kirchner J. Evolutionary dynamics of pathogen resistance and tolerance.
570 *Evolution*. 2000;54(1):51–63.
- 571 Ryder JJ, Miller MR, White A, Knell RJ, Boots M. Host-parasite population
572 dynamics under combined frequency-and density-dependent transmission. *Oikos*.

573 2007;116(12):2017–2026.

574 Råberg L, Sim D, Read AF. Disentangling genetic variation for resistance and
575 tolerance to infectious diseases in animals. *Science*. 2007;318(5851):812–814.

576 Shaw AK, Craft ME, Zuk M, Binning SA. Host migration strategy is shaped by
577 forms of parasite transmission and infection cost. *Journal of Animal Ecology*.
578 2019;88(10):1601–1612.

579 Smith MJ, Telfer S, Kallio ER, Burthe S, Cook AR, Lambin X, et al. Host-
580 pathogen time series data in wildlife support a transmission function between
581 density and frequency dependence. *Proceedings of the National Academy of
582 Sciences*. 2009;106(19):7905–7909.

583 Sutherland C, Elston D, Lambin X. A demographic, spatially explicit patch occupancy
584 model of metapopulation dynamics and persistence. *Ecology*. 2014;95(11):3149–
585 3160.

586 Szilágyi A, Meszéna G. Two-patch model of spatial niche segregation. *Evolutionary
587 Ecology*. 2009;23(2):187–205.

588 Thrall PH, Antonovics J, Hall DW. Host and pathogen coexistence in sexually
589 transmitted and vector-borne diseases characterized by frequency-dependent disease
590 transmission. *The American Naturalist*. 1993;142(3):543–552.

591 Turner PE, Cooper VS, Lenski RE. Tradeoff between horizontal and vertical modes
592 of transmission in bacterial plasmids. *Evolution*. 1998;52(2):315–329.

593 Xia Y, Bjørnstad ON, Grenfell BT. Measles metapopulation dynamics: a grav-
594 ity model for epidemiological coupling and dynamics. *The American Naturalist*.
595 2004;164(2):267–281.

596 Zeng Q, Yu X, Ni H, Xiao L, Xu T, Wu H, et al. Dengue transmission dynamics
597 prediction by combining metapopulation networks and Kalman filter algorithm.

598 PLOS Neglected tropical diseases. 2023;17(6):e0011418.

599 Zilio G, Thiévent K, Koella JC. Host genotype and environment affect the trade-off
600 between horizontal and vertical transmission of the parasite *Edhazardia aedis*. BMC
601 evolutionary biology. 2018;18:1–9.

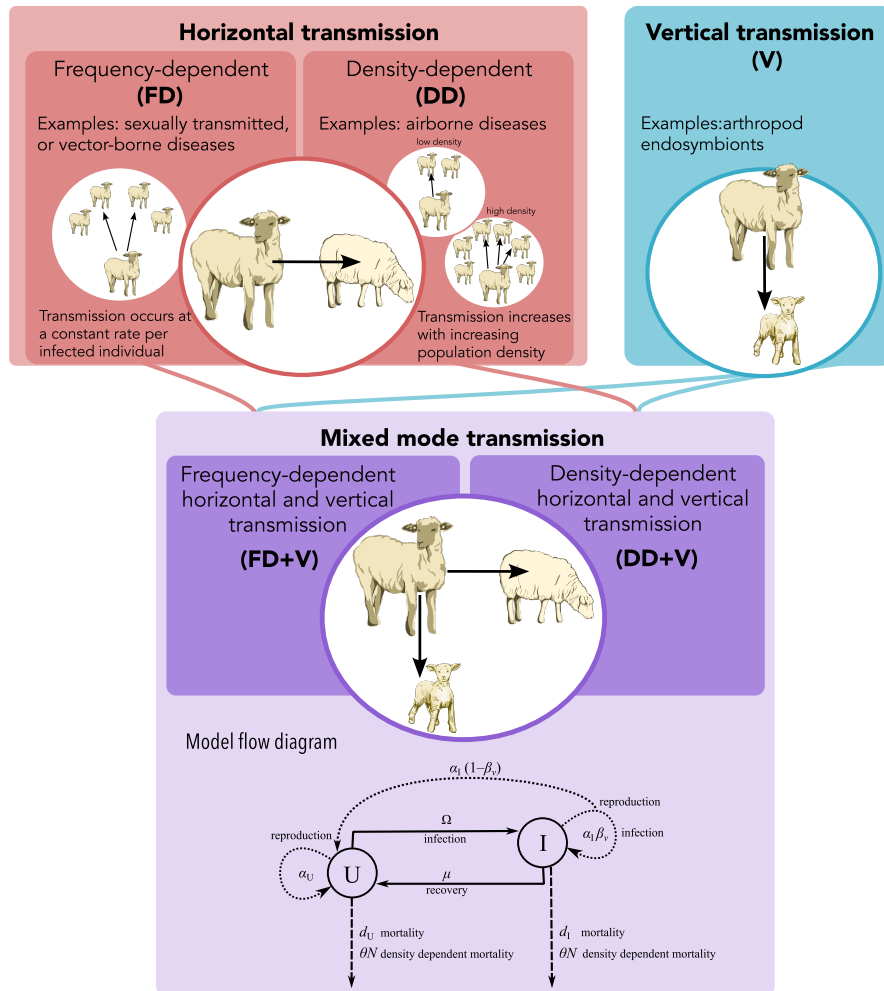


Fig. 1 Overview of the different transmission modes (and combinations thereof) considered. Transmission modes are broadly classified as horizontal (red box) or vertical (blue box). In the former, diseases transmit between two distinct individuals that are not necessarily related, while the latter specifies that transmission occurs from parent to offspring. Some diseases utilize both modes to infect new hosts, which is usually referred to as mixed-mode transmission (purple box). The five distinct cases shown are: frequency-dependent horizontal transmission (FD), density-dependent horizontal transmission (DD), vertical transmission (V), mixed mode transmission (FD+V), with frequency-dependent horizontal and vertical transmission and mixed mode transmission (DD+V), with density-dependent horizontal and vertical transmission. At the bottom is a flow diagram corresponding to the presented model of mixed-mode transmission (equation 1). Meanings of the symbols are listed in Table 1. Solid lines correspond to infection gain or loss, while dashed lines mark mortality and dotted lines show processes corresponding to reproduction.

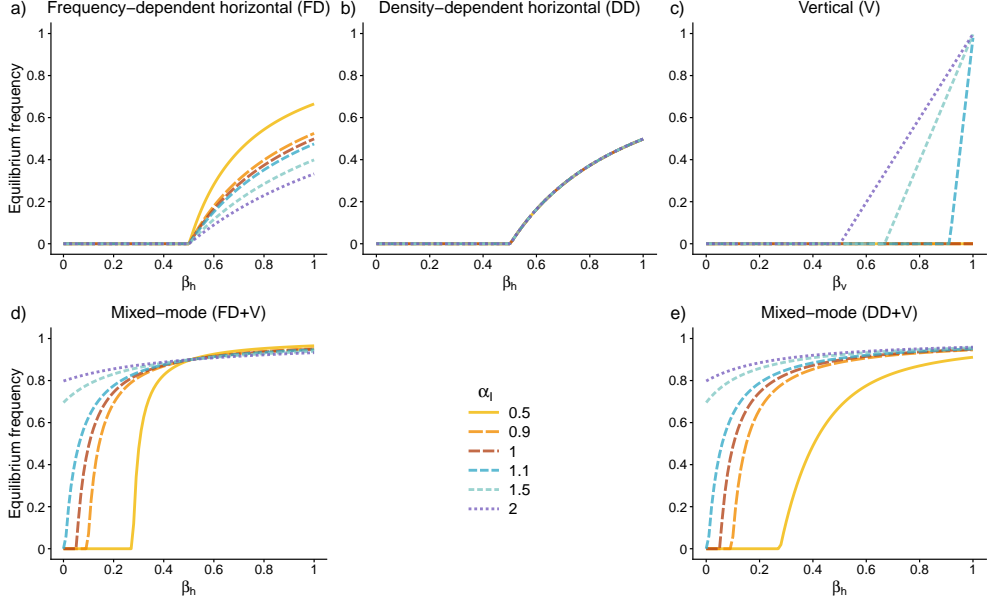


Fig. 2 Change in equilibrium frequency of infected individuals \hat{I} with parasite transmission efficiency β and different per capita birth rate for infected individuals α_I for the different transmission mode scenarios: a) frequency-dependent horizontal transmission, b) density-dependent horizontal transmission, c) vertical transmission, d) mixed-mode transmission with frequency-dependent horizontal and vertical transmission and e) mixed-mode transmission with density-dependent horizontal and vertical transmission. Parameter values: $\alpha_U = 1$, $\mu = 0.002$, $d_U = 0.001$, $d_I = 0.002$, $\theta = 0.001$. The contact rate c was adjusted for the different cases of horizontal transmission. In a) and d) $c = 2$, while in b) and e) $c = 0.002$. In the mixed-mode transmission scenarios vertical transmission efficiency is set to $t_v = 0.9$. Population is initialized with $I = 1$ and $U = 199$.

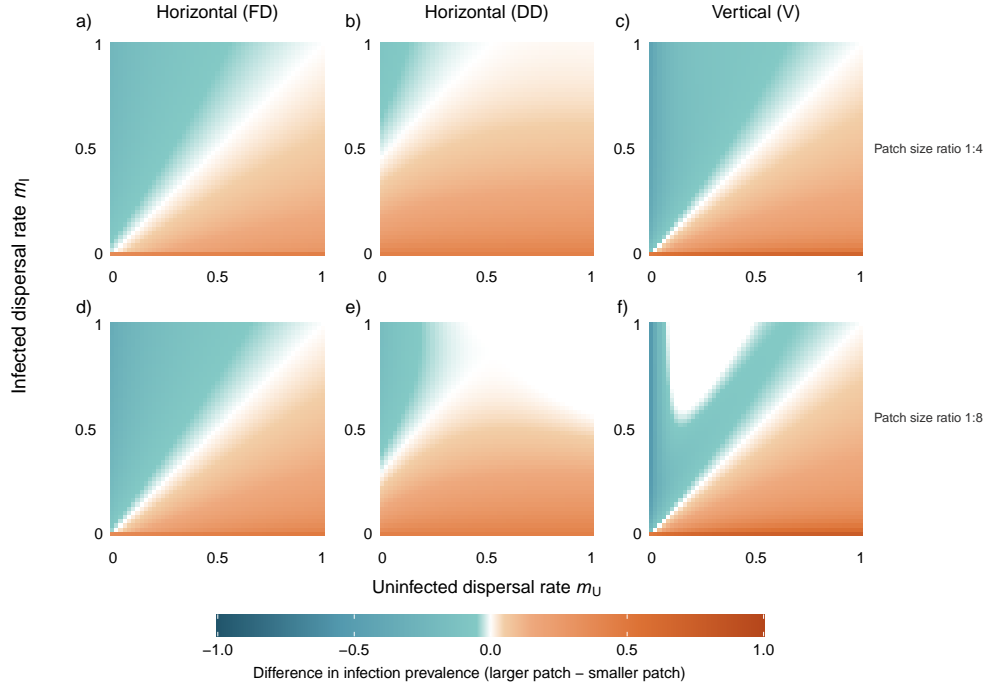


Fig. 3 Infection prevalence difference between two patches for varying dispersal rates, patch size ratios and transmission modes. Heatmap color shows the difference in infection prevalence between two patches (larger patch - smaller patch), where negative values indicate comparatively higher infection prevalence in the smaller patch, while positive values correspond to the larger patch containing higher infection prevalence. The parasite can transmit via frequency-dependent horizontal (a,d), density-dependent horizontal (b,e) or vertical transmission (c,f) modes. The difference in patch size is 1:4 ($\theta_{large} = 0.001$, $\theta_{small} = 0.004$) in the top row (a-c) and 1:8 ($\theta_{large} = 0.001$, $\theta_{small} = 0.008$) in the bottom row (d-f). Other parameters used: $\alpha_U = 1.04$, $\alpha_I = 1.3$, $d_U = 0.001$, $d_I = 0.002$, $\beta_h = 0.9$, $\beta_v = 0.9$, $c_{FD} = 2$, $c_{DD} = 0.0035$ and $\mu = 0.002$.

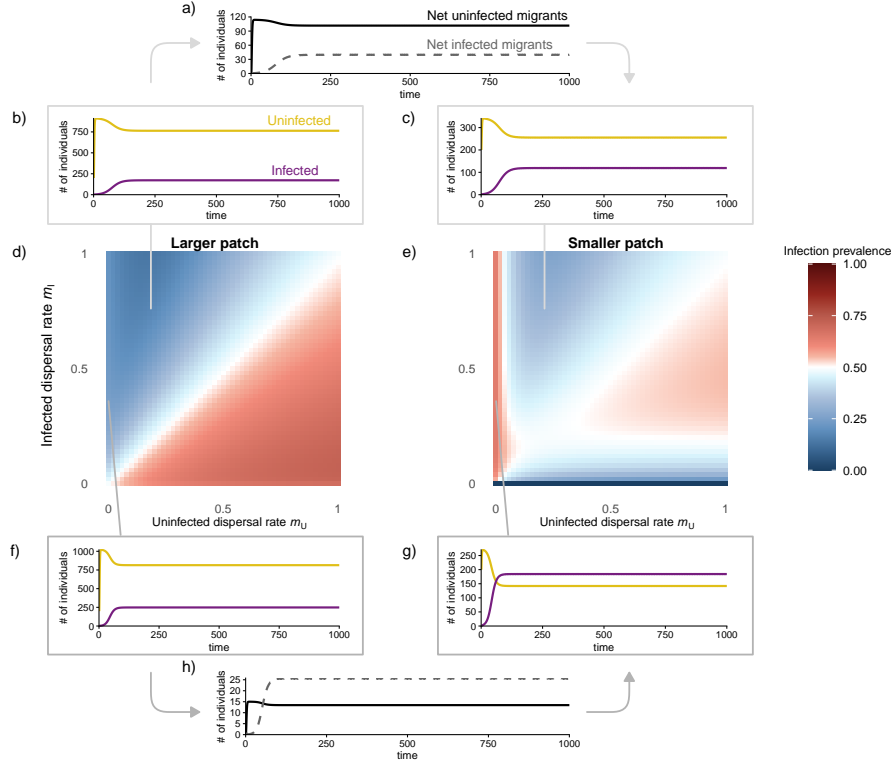


Fig. 4 Spread of a vertically transmitted parasite in two connected patches depending on dispersal rate of infected and uninfected individuals. Heatmap colors indicate infection prevalence in the larger $\theta_{large} = 0.001$ (d) and smaller patch $\theta_{small} = 0.004$ (e). The top grey boxes (a,c) exemplify the dynamics within each patch when uninfected and infected individuals disperse at rate $m_U = 0.2$ and $m_I = 0.75$, respectively. Due to the patch size difference (1:4), the smaller patch gains a net positive number of migrants (a), while the larger patch suffers the proportional net migration loss. Dispersal rates of $m_U = 0.02$ and $m_I = 0.4$ (bottom grey boxes; f,g), similarly produce a net positive migration from the larger to the smaller patch. Here, infected individuals disperse at a sufficiently high rate to outnumber the less dispersive uninfected migrants (h), resulting in a higher infection prevalence in the smaller compared to the larger patch (d,e,f,g). Other parameters: $\alpha_U = 1.04$, $\alpha_I = 1.3$, $d_U = 0.001$, $d_I = 0.002$, $\beta_h = 0.9$, $\beta_v = 0.9$, $c_{FD} = 2$, $c_{DD} = 0.002$ and $\mu = 0.002$.

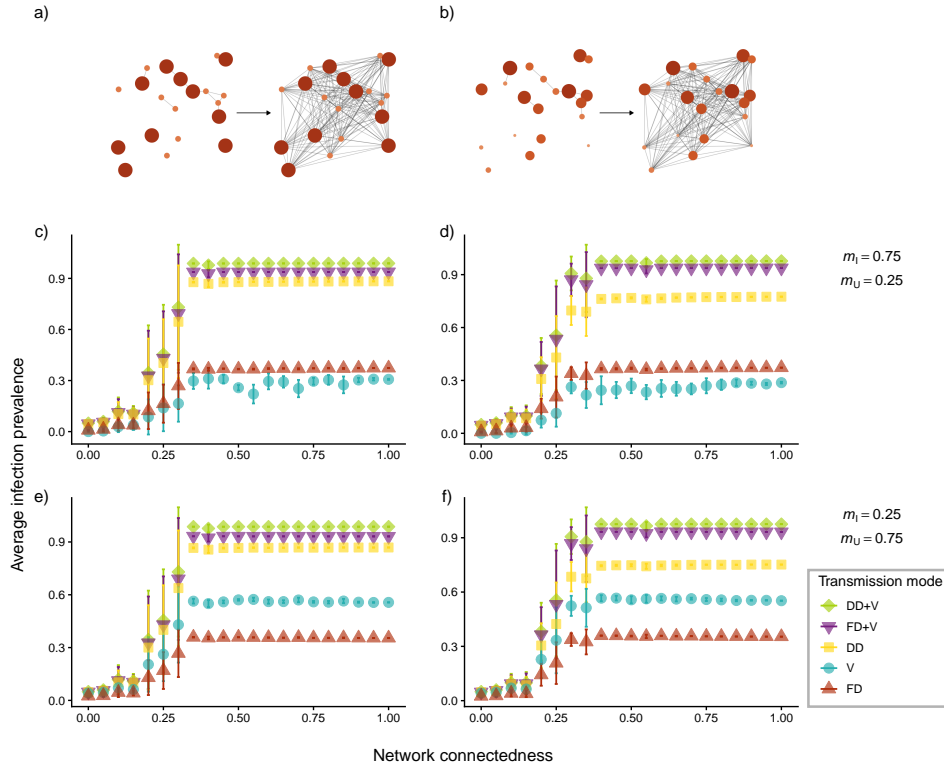


Fig. 5 Impact of transmission mode on global infection prevalence in randomly generated networks. We generate networks of 20 patches with distinct patch size configurations. Examples of such networks are shown for low levels of patch connectedness (left) to maximum connectedness $a = 1$ (right) (a,b). Patch size ratios were either 1:5 (where half of the patches are five times smaller than the other half, $\theta_{larger} = 0.001$ and $\theta_{smaller} = 0.005$) (a,c,e) or 1:10 (where patch sizes gradually decrease up to ten times smaller than the largest patches with two patches of each size, $\theta_n = 0.001n$ for $n = 1 : 10$) (b,d,f). For each network, we track the global infection prevalence after 1000 timesteps for all parasite transmission modes (c-f), while also varying connectedness a of the patches. Calculations were repeated for five different randomly generated networks, with all transmission modes applied to each created network. This procedure was replicated for different dispersal propensities with $m_I = 0.75$ and $m_U = 0.25$ (c,d) and $m_I = 0.25$ and $m_U = 0.75$ (e,f). Other parameters: $\alpha_U = 1.04$, $\alpha_I = 1.3$, $d_U = 0.001$, $d_I = 0.002$, $\beta_h = 0.9$, $\beta_v = 0.9$, $c_{FD} = 2$, $c_{DD} = 0.02$ and $\mu = 0.002$.

602 **Supplementary Information**

603 **S1 Single patch dynamics**

604 We first denote the UIU (uninfected-infected-uninfected) model for a well mixed pop-
 605 ulation of asexually reproducing hosts. To compare infection dynamics resulting from
 606 five distinct transmission modes, we develop five separate models, each corresponding
 607 to a parasite using a different mode of transmission. We are not explicitly modeling
 608 parasite dynamics, but define a population of N host individuals, that can be infected
 609 I or uninfected U . Thus, $N = U + I$.

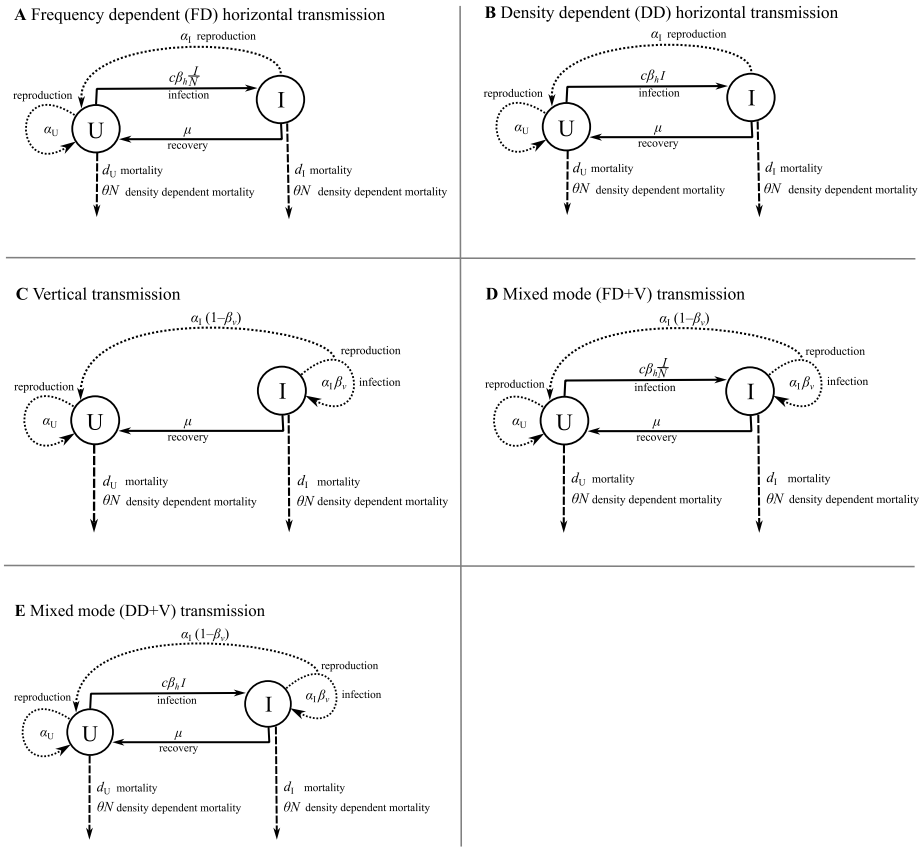


Fig. S1 Flow diagram corresponding to each considered transmission mode. Meaning of symbols are listed in Table 1. Solid lines correspond to parasite gain or loss, while dashed lines mark mortality and dotted lines show processes corresponding to reproduction.

610 **S1.1 Horizontal transmission**

611 **S1.1.1 Frequency-dependent horizontal transmission**

612 In sexually transmitted or vector borne diseases, horizontal transmission is commonly
613 described as frequency-dependent (FD). The underlying assumption is that the par-
614 asite transmits at a constant rate per infected individual in the population, as is the
615 case with sexual contacts or bites from a vector species that occur at a stable rate
616 per infected individual. We denote the infection dynamics of a frequency-dependent
617 horizontally transmitted parasite in a single well mixed host environment as

$$\begin{aligned}\frac{dU}{dt} &= \alpha_U U + \alpha_I I + \mu I - c\beta_h \frac{I}{N} U - d_U U - \theta N U, \\ \frac{dI}{dt} &= c\beta_h \frac{I}{N} U - \mu I - d_I I - \theta N I.\end{aligned}\tag{S1}$$

618 Here, α is the per capita growth rate and d the baseline mortality for uninfected
619 and infected individuals, as indicated by the subscript $_U$ and $_I$, respectively. We
620 assume that both fertility and mortality can differ with infection state, as infected
621 individuals may experience higher mortality and reduced fertility compared to healthy
622 con-specifics. The entire population is subject to the same density-dependent mortal-
623 ity, where increased crowding in the environment results in higher mortality. This effect
624 is scaled by the parameter θ , modulating the strength of density-dependent mortality
625 in a population. Individuals encounter one another at contact rate c , and the proba-
626 bility of coming into contact with an infected individual is given by the frequency of
627 infected individuals in the population $\frac{I}{N}$. Upon contact with an infected individual,
628 horizontal transmission of the parasite occurs with transmission efficiency β_h , resulting
629 in infection of a previously uninfected individual. Infected individuals can recover and
630 rejoin the uninfected state at recovery rate μ . See figure S1a for a flow diagram corre-
631 sponding to equations (S1), and Table 1 for a list of all symbols. Using equations 1,
632 we can derive two different equilibrium states for the infection dynamics. In the first,

633 infection does not spread and the population consists of uninfected individuals:

$$\begin{aligned}\hat{U} &= \frac{\alpha_U - d_U}{\theta} \\ \hat{I} &= 0.\end{aligned}\tag{S2}$$

634 In the second, infected individuals spread in the population and reach a stable
635 equilibrium with

$$\begin{aligned}\hat{U} &= -\frac{(\alpha_I - \mu)(-d_U^2 - c\beta_h\alpha_I + d_I(c\beta_h - \alpha_U + \alpha_I - \mu) - \alpha_U\mu + \alpha_I\mu + d_U(d_I + \mu))}{(d_U - d_I + c\beta_h - \alpha_U + \alpha_I)^2\theta} \\ \hat{I} &= -\frac{(d_U - d_I + c\beta_h - \alpha_U - \mu)(-d_I^2 - c\beta_h\alpha_I + d_I(c\beta_h - \alpha_U + \alpha_I - \mu) - \alpha_U\mu + \alpha_I\mu + d_U(d_I + \mu))}{(d_U - d_I + c\beta_h - \alpha_U + \alpha_I)^2\theta}.\end{aligned}\tag{S3}$$

636 Note how no trivial equilibrium exists, because when $I = 0$ and $U = 0$, it results
637 that $N = U + I = 0$ and then $\frac{I}{N} = \frac{0}{0}$, which does not yield meaningful results. Thus,
638 the system is not defined at point $(0,0)$. For an example of the resulting dynamics of
639 the system, see the corresponding phase portrait (Figure S2).

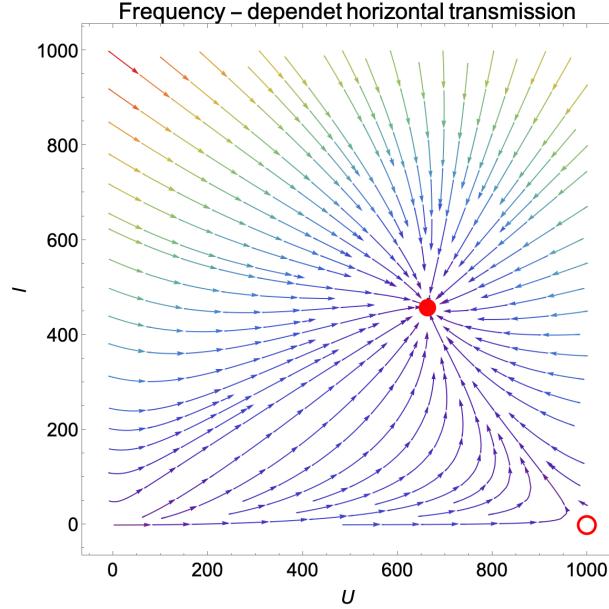


Fig. S2 Phase portrait with stability markers (red circles) for equilibria. The filled circle corresponds to the stable, the open circle to the unstable equilibrium calculated with parameters $\alpha_U = 1$, $\alpha_I = 1.3$, $d_U = 0.001$, $d_I = 0.002$, $\beta_h = 0.95$, $c = 2$, $\mu = 0.00003$ and $\theta = 0.001$.

640 **S1.1.2 Density-dependent horizontal transmission**

641 Compared to frequency-dependent transmission, density-dependent (DD) horizontal
 642 transmission captures the dynamics of parasites whose infectiousness increases with
 643 the density of individuals in an area. This is the case, for example, in diseases that are
 644 airborne or waterborne. We define the infection dynamics for such a case in a single
 645 patch as

$$\begin{aligned}\frac{dU}{dt} &= \alpha_U U + \alpha_I I + \mu I - c\beta_h IU - d_U U - \theta NU, \\ \frac{dI}{dt} &= c\beta_h IU - \mu I - d_I I - \theta NI.\end{aligned}\tag{S4}$$

646 Transmission of infection rises as population density increases (density-dependent or
 647 mass-action infection). Thus, the chance of a new infection is proportional to the
 648 number of infected and uninfected individuals in the population IU and scaled by the
 649 contact rate and transmission efficiency of the parasite $c\beta_h$. All other symbols and
 650 dynamics are identical to the frequency-dependent case. See the complementary flow
 651 diagram in figure S1b and Table 1 for a list of all symbols. For this system of equations,
 652 we can derive four different equilibrium states. In addition to the trivial equilibrium
 653 ($\hat{U} = 0, \hat{I} = 0$), there are three more equilibrium points:

$$\begin{aligned}\hat{U} &= \frac{\alpha_U - d_U}{\theta}, \\ \hat{I} &= 0,\end{aligned}\tag{S5}$$

654

$$\begin{aligned}\hat{U} &= \frac{1}{2c^2\beta_h^2} \left((-d_U + d_I + \alpha_U - \alpha_I)\theta + c\beta_h(d_I + \alpha_I + 2\mu) - A, \right. \\ \hat{I} &= \frac{1}{2c^2\beta_h^2\theta} \left(c^2\beta_h^2(-d_I + \alpha_I) + (d_U - d_I - \alpha_U + \alpha_I)\theta^2 \right. \\ &\quad \left. \left. - c\beta_h\theta(d_U - \alpha_U + 2(\alpha_I + \mu)) - c\beta_h A + \theta A \right),\end{aligned}\tag{S6}$$

655 and

$$\begin{aligned}\hat{U} &= \frac{1}{2c^2\beta_h^2} \left((-d_U + d_I + \alpha_U - \alpha_I)\theta + c\beta_h(d_I + \alpha_I + 2\mu) + A, \right. \\ \hat{I} &= \frac{1}{2c^2\beta_h^2\theta} \left(c^2\beta_h^2(-d_I + \alpha_I) + (d_U - d_I - \alpha_U + \alpha_I)\theta^2 \right. \\ &\quad \left. \left. - c\beta_h\theta(d_U - \alpha_U + 2(\alpha_I + \mu)) + c\beta_h A - \theta A \right),\end{aligned}\tag{S7}$$

656 with $A = \sqrt{-4c^2\beta_h^2(d_I + \mu)(\alpha_I + \mu) + ((-d_U + d_I + \alpha_U - \alpha_I)\theta + c\beta_h(d_I + \alpha_I + 2\mu))^2}$.
 657 See Figure S3 for a example of a corresponding phase portrait.

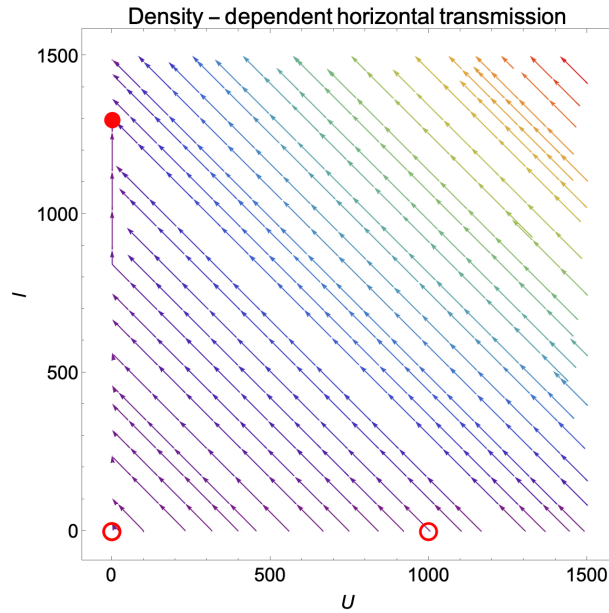


Fig. S3 Phase portrait with stability markers (red circles) for equilibria. The filled circle corresponds to the stable, the open circles to the unstable equilibrium calculated with parameters $\alpha_U = 1$, $\alpha_I = 1.3$, $d_U = 0.001$, $d_I = 0.002$, $\beta_h = 0.95$, $c = 2$, $\mu = 0.00003$ and $\theta = 0.001$. Note how the trivial equilibrium point is closely spaced with another equilibrium point, making the circles visually overlap and appear as a single circle.

658 S1.2 Vertical transmission

659 In this section, we consider the vertical transmission of a parasite in a host population.
 660 Examples of parasites that can transmit vertically include *Herpes simplex* virus and
 661 various endosymbionts inhabiting arthropods like *Wolbachia*. While the first example
 662 does not transmit only through the vertical mode, *Wolbachia* predominantly relies on
 663 vertical transmission. We define the infection dynamics with a parasite that exclusively

664 transmits vertically as

$$\begin{aligned}\frac{dU}{dt} &= \alpha_U U + \alpha_I(1 - \beta_v)I + \mu I - d_U U - \theta NU, \\ \frac{dI}{dt} &= \alpha_I \beta_v I - \mu I - d_I I - \theta NI.\end{aligned}\tag{S8}$$

665 Because transmission of the parasite is exclusively vertical, we assume that only
 666 infected individuals can birth infected individuals and thus, uninfected individuals
 667 cannot acquire the infection throughout their life. Vertical transmission efficiency is
 668 denoted by β_v , representing the proportion of offspring that inherit the parasite from
 669 an infected parent. The remaining proportion $1 - \beta_v$ consists of offspring that did not
 670 inherit the parasite due to transmission failure and is instead added to the number of
 671 uninfected individuals in the population. Infected individuals can recover and lose the
 672 infection at rate μ , equivalent to the assumption in the previously described cases of
 673 horizontal transmission. All other dynamics are identical to the scenarios with hori-
 674 zontal transmission. See figure S1c for a flow diagram corresponding to equations S8
 675 and Table 1 for a list of all symbols. Equations S8 yield three equilibrium states. In
 676 addition to the a trivial equilibrium point, we can determine two more equilibria of
 677 the population:

$$\begin{aligned}\hat{U} &= \frac{\alpha_U - d_U}{\theta}, \\ \hat{I} &= 0\end{aligned}\tag{S9}$$

678 and

$$\begin{aligned}\hat{U} &= \frac{((-1 + \beta_v)\alpha_I - \mu)(d_I - \beta_v\alpha_I + \mu)}{(d_U - d_I - \alpha_U + \alpha_I)\theta}, \\ \hat{I} &= -\frac{(d_U - d_I - \alpha_U + \beta_v\alpha_I - \mu)(d_I - \beta_v\alpha_I + \mu)}{(d_U - d_I - \alpha_U + \alpha_I)\theta}.\end{aligned}\tag{S10}$$

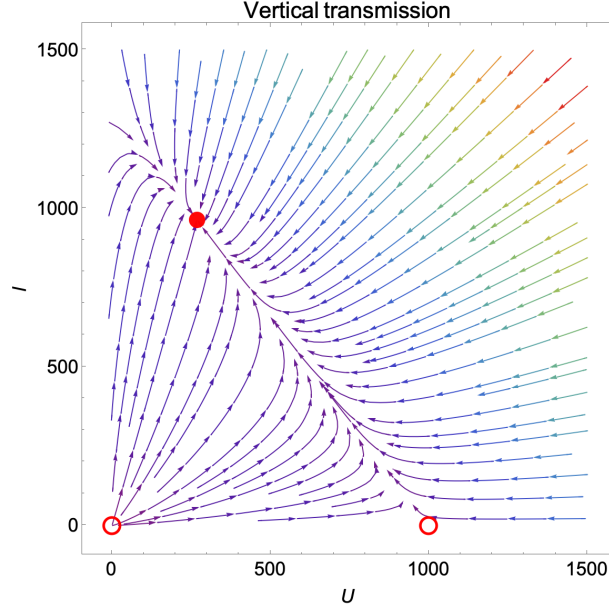


Fig. S4 Phase portrait with stability markers (red circles) for equilibria. The filled circle corresponds to the stable, the open circles to the unstable equilibrium calculated with parameters $\alpha_U = 1$, $\alpha_I = 1.3$, $d_U = 0.001$, $d_I = 0.002$, $\beta_v = 0.95$, $\mu = 0.00003$ and $\theta = 0.001$.

679 **S1.3 Mixed mode transmission (horizontal and vertical)**

680 **S1.3.1 frequency-dependent horizontal and vertical transmission** 681 **(FD+V)**

682 Some parasites are able to transmit via multiple modes, usually referred to as mixed-
683 mode transmission. We consider parasites with mixed-mode transmission that utilize
684 both a horizontal and a vertical pathway. We first denote the infection dynamics for
685 a parasite that combines frequency-dependent horizontal and vertical transmission as

$$\begin{aligned} \frac{dU}{dt} &= \alpha_U U + \alpha_I (1 - \beta_v) I + \mu I - d_U U - \theta N U - c \beta_h \frac{I}{N} U, \\ \frac{dI}{dt} &= \alpha_I \beta_v I + c \beta_h \frac{I}{N} U - \mu I - d_I I - \theta N I. \end{aligned} \quad (\text{S11})$$

686 Here, parasites can transmit both horizontally and vertically, though transmission effi-
687 ciency may vary by mode. It is possible that horizontal and vertical transmission are

688 equally efficient ($\beta_h = \beta_v$), or that transmission efficiency is higher via one mode com-
 689 pared to the other $\beta_h < \beta_v$ or $\beta_h > \beta_v$. Individuals can inherit the parasite (vertical)
 690 or get infected during their life (horizontal). All other dynamics mirror the previous
 691 equations considering parasites with a single transmission mode. See figure S1d for a
 692 flow diagram corresponding to equations S11, Table 1 for a list of all symbols. Similar
 693 to the scenario with only frequency-dependent horizontal transmission, in this mixed-
 694 mode transmission case, there is no trivial equilibrium, because the system cannot be
 695 defined when $\frac{I}{N} = \frac{0}{0}$. The equilibrium points of the system are

$$\begin{aligned}
 \hat{U} &= \frac{\alpha_U - d_U}{\theta}, \\
 \hat{I} &= 0
 \end{aligned}
 \tag{S12}$$

696 and

$$\begin{aligned}
 \hat{U} &= \frac{1}{(d_U - d_I + c\beta_h - \alpha_U + \alpha_I)^2 \theta} (((\beta_v - 1)\alpha_I - \mu)C), \\
 \hat{I} &= -\frac{1}{(d_U - d_I + c\beta_h - \alpha_U + \alpha_I)^2 \theta} (d_U - d_I + c\beta_h - \alpha_U + \beta_v \alpha_I - \mu)C
 \end{aligned}
 \tag{S13}$$

697 with $C = (-d_I^2 - \alpha_I(c\beta_h - \beta_v \alpha_U + \beta_v \alpha_I) + d_I(c\beta_h - \alpha_U + \alpha_I + \beta_v \alpha_I - \mu) + (\alpha_I - \alpha_U)\mu + d_U(d_I - \beta_v \alpha_I + \mu))$.

698 See Figure S5 for a corresponding phase portrait.

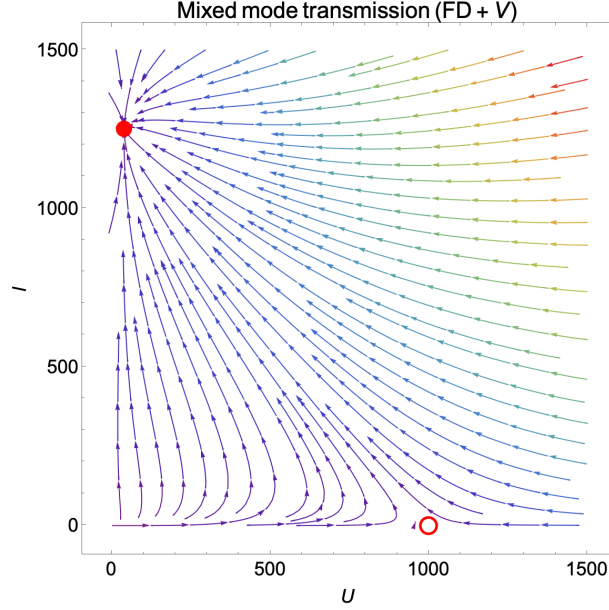


Fig. S5 Phase portrait with stability markers (red circles) for equilibria. The filled circle corresponds to the stable, the open circles to the unstable equilibrium calculated with parameters $\alpha_U = 1$, $\alpha_I = 1.3$, $d_U = 0.001$, $d_I = 0.002$, $\beta_h = 0.95$, $\beta_v = 0.95$, $c = 2$, $\mu = 0.00003$ and $\theta = 0.001$.

699 **S1.3.2 Density-dependent horizontal and vertical transmission**
700 **(DD+V)**

701 Next, we define the infection dynamics for a parasite that uses a combination of
702 density-dependent horizontal and vertical transmission as

$$\begin{aligned}\frac{dU}{dt} &= \alpha_U U + \alpha_I (1 - \beta_v) I + \mu I - d_U U - \theta N U - c \beta_h I U, \\ \frac{dI}{dt} &= \alpha_I \beta_v I + c \beta_h I U - \mu I - d_I I - \theta N I.\end{aligned}\tag{S14}$$

703 All symbols (Table 1) and assumptions follow the previous cases. See figure S1e for
704 a flow diagram corresponding to equations S14. We derive four equilibrium points
705 (Figure S6) for this system of equations. One is trivial, the others are:

$$\begin{aligned}\hat{U} &= \frac{\alpha_U - d_U}{\theta}, \\ \hat{I} &= 0,\end{aligned}\tag{S15}$$

$$\begin{aligned}\hat{U} &= \frac{1}{2c^2\beta_h^2} \left(cd_I\beta_h + c\beta_h\alpha_I - 2c\beta_h\beta_v\alpha_I - d_U\theta + d_I\theta + \alpha_U\theta - \alpha_I\theta + 2c\beta_h\mu - B \right), \\ \hat{I} &= \frac{1}{2c^2\beta_h^2\theta} \left(-c^2d_I\beta_h^2 + c^2\beta_h^2\alpha_I - cd_U\beta_h\theta + c\beta_h\alpha_U\theta - 2c\beta_h\alpha_I\theta + 2c\beta_h\beta_v\alpha_I\theta \right. \\ &\quad \left. + d_U\theta^2 - d_I\theta^2 - \alpha_U\theta^2 + \alpha_I\theta^2 - 2c\beta_h\theta\mu - c\beta_hB + \theta B \right).\end{aligned}\tag{S16}$$

706 and

$$\begin{aligned}\hat{U} &= \frac{1}{2c^2\beta_h^2} \left(cd_I\beta_h + c\beta_h\alpha_I - 2c\beta_h\beta_v\alpha_I - d_U\theta + d_I\theta + \alpha_U\theta - \alpha_I\theta + 2c\beta_h\mu + B \right), \\ \hat{I} &= \frac{1}{2c^2\beta_h^2\theta} \left(-c^2d_I\beta_h^2 + c^2\beta_h^2\alpha_I - cd_U\beta_h\theta + c\beta_h\alpha_U\theta - 2c\beta_h\alpha_I\theta + 2c\beta_h\beta_v\alpha_I\theta \right. \\ &\quad \left. + d_U\theta^2 - d_I\theta^2 - \alpha_U\theta^2 + \alpha_I\theta^2 - 2c\beta_h\theta\mu + c\beta_hB - \theta B \right)\end{aligned}\tag{S17}$$

707 with $B = \sqrt{4c^2\beta_h^2((-1 + \beta_v)\alpha_I - \mu)(d_I - \beta_v\alpha_I + \mu) + ((-d_U + d_I + \alpha_U - \alpha_I)\theta + c\beta_h(d_I + \alpha_I - 2\beta_v\alpha_I + 2\mu))^2}$.

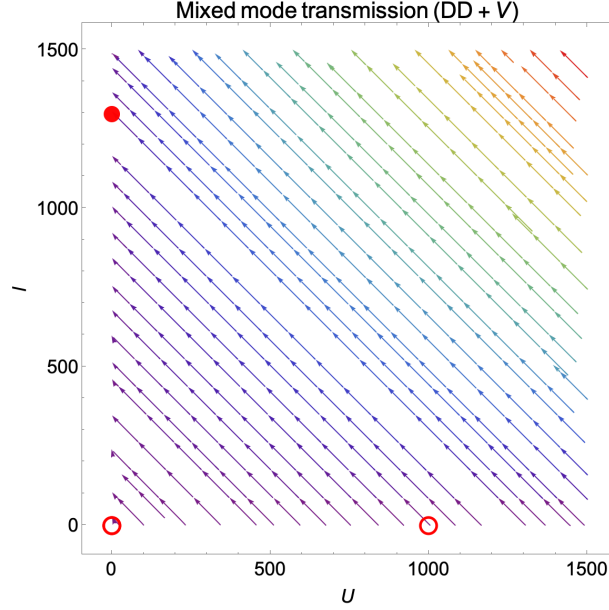


Fig. S6 Phase portrait with stability markers (red circles) for equilibria. The filled circle corresponds to the stable, the open circles to the unstable equilibrium calculated with parameters $\alpha_U = 1$, $\alpha_I = 1.3$, $d_U = 0.001$, $d_I = 0.002$, $\beta_h = 0.95$, $\beta_v = 0.95$, $c = 2$, $\mu = 0.00003$ and $\theta = 0.001$. Note how the trivial equilibrium point is closely spaced with another equilibrium point, making the circles visually overlap and appear as a single circle.

708 S2 Mainland-island models

709 As an example, consider 2 patches i and j , where dispersal from i to j is just as likely
 710 as dispersal from j to i , meaning that the habitats are equally well connected. This
 711 symmetrical connectedness is captured by the connection matrix \mathbf{S} below.

$$\mathbf{S} = \begin{bmatrix} -1 & 1 \\ 1 & -1 \end{bmatrix} \quad (\text{S18})$$

712 The elements of the matrix, s_{ij} , describes the proportion of dispersers from
 713 patch i that relocate to patch j . For the connection matrix above (equation S18)
 714 $s_{1,2} = s_{2,1} = 1$, meaning that all dispersing individuals of patch 1 move to patch
 715 2 and vice versa. The diagonal elements in matrix \mathbf{S} captures the corresponding
 716 emigration of dispersers from each patch with $s_{ii} = -1$, $i = 1, 2$, indicating that all

717 dispersers from i successfully leave patch i .

718

719 In our model we consider that infection state can influence dispersal propensity.
720 Infected individuals, for example, may become more or less likely to move to a new
721 patch compared to uninfected con-specifics (insert REF). To account for this, we define
722 two different dispersal propensities m_U and m_I , referring to uninfected and infected
723 individuals, respectively. Matrix \mathbf{M} tracks the dispersal probability of different types
724 of individuals:

$$\mathbf{M} = \begin{bmatrix} m_U & 0 \\ 0 & m_I \end{bmatrix} \quad (\text{S19})$$

725

726 Here, $m_{1,2} = 0$ and $m_{2,1} = 0$ (equation S19) further implies that individuals cannot
727 get infected or recover during dispersal, which underlines our model assumption that
728 infection status can only change within the dynamics of a patch.

729

730 To evaluate the possibility that two habitats are of different sizes, we assign patch
731 specific density-dependent mortality θ_i , θ_j . A larger density-dependent mortality θ ,
732 corresponds to a smaller habitat, where individual mortality increases at compara-
733 tively lower levels of crowding. Note that this form of population size regulation does
734 not impose a strict carrying capacity. Instead, the penalty for crowding increases
735 with larger population size θN . Here we explicitly note down the equations for the
736 two-patch dynamics between patch i and j .

737

738 In the following, we denote the equations for each transmission mode (equations S1,
739 S4, S8, S11 and S14) and expand them to a two-patch system, as described above,
740 where two habitats are connected by dispersing individuals.

741 **S2.1 Frequency-dependent horizontal transmission and in a**
742 **two-patch system**

743 In the FD horizontal transmission scenario, in a world with two equally well connected
744 patches j and i equation 1 boils down to:

$$\begin{aligned}
\frac{dU_j}{dt} &= \alpha_U U_j + \alpha_I I_j + \mu I_j - \theta_j N_j U_j - c\beta_h \frac{I_j}{N_j} U_j - d_U U_j + m_U (U_i - U_j), \\
\frac{dI_j}{dt} &= c\beta_h \frac{I_j}{N_j} U_j - \theta_j N_j I_j - \mu I_j - d_I I_j + m_I (I_i - I_j), \\
\frac{dU_i}{dt} &= \alpha_U U_i + \alpha_I I_i + \mu I_i - \theta_i N_i U_i - c\beta_h \frac{I_i}{N_i} U_i - d_U U_i + m_U (U_j - U_i), \\
\frac{dI_i}{dt} &= c\beta_h \frac{I_i}{N_i} U_i - \theta_i N_i I_i - \mu I_i - d_I I_i + m_I (I_j - I_i).
\end{aligned} \tag{S20}$$

745 **S2.2 Density-dependent horizontal transmission and in a**
746 **two-patch system**

747 Now we repeat these considerations for density-dependent horizontal transmission.
748 However, we now note down the dynamics for only one patch in the two-patch system,
749 as the equations are equivalent for the second patch, expect for swapped indices i for
750 j and vice versa:

$$\begin{aligned}
\frac{dU_j}{dt} &= \alpha_U U_j + \alpha_I I_j + \mu I_j - \theta_j N_j U_j - c\beta_h I_j U_j - d_U U_j + m_U (U_i - U_j), \\
\frac{dI_j}{dt} &= c\beta_h I_j U_j - \theta_j N_j I_j - \mu I_j - d_I I_j + m_I (I_i - I_j).
\end{aligned} \tag{S21}$$

751 This describes the change in frequency of infected and susceptible individuals in
752 patches i and j .

753

754 **S2.3 Vertical transmission and in a two-patch system**

755 We can derive the dynamics when the parasite is transmitted exclusively vertically
756 (written down as an example in just one patch, dynamics in the second patch are

757 equivalent but with swapped i and j):

$$\begin{aligned}\frac{dU_j}{dt} &= \alpha_U U_j + \alpha_I(1 - \beta_v)I_j + \mu I_j - \theta_j N_j U_j - d_U U_j + m_U(U_i - U_j), \\ \frac{dI_j}{dt} &= \alpha_I \beta_v I_j - \theta_j N_j I_j - \mu I_j - d_I I_j + m_I(I_i - I_j),\end{aligned}\tag{S22}$$

758 **S2.4 Mixed-mode transmission (FD+V) and in a two-patch**
759 **system**

760 For mixed-mode (FD+V) transmission of the parasite, the equations to describe the
761 dynamics in the different patches are:

$$\begin{aligned}\frac{dU_j}{dt} &= \alpha_U U_j + \alpha_I(1 - \beta_v)I_j + \mu I_j - \theta_j N_j U_j - c\beta_h \frac{I_j}{N_j} U_j - d_U U_j + m_U(U_i - U_j), \\ \frac{dI_j}{dt} &= \alpha_I \beta_v I_j + c\beta_h \frac{I_j}{N_j} U_j - \theta_j N_j I_j - \mu I_j - d_I I_j + m_I(I_i - I_j).\end{aligned}\tag{S23}$$

762 The dynamics in the second patch are equivalent but with swapped i and j .

763

764 **S2.5 Mixed-mode transmission and in a two-patch system**

765 Lastly, in the case of mixed-mode transmission with density-dependent horizontal and
766 vertical transmission the two patch dynamics can be denoted as:

$$\begin{aligned}\frac{dU_j}{dt} &= \alpha_U U_j + \alpha_I(1 - \beta_v)I_j + \mu I_j - \theta_j N_j U_j - c\beta_h I_j U_j - d_U U_j + m_U(U_i - U_j), \\ \frac{dI_j}{dt} &= \alpha_I \beta_v I_j + c\beta_h I_j U_j - \theta_j N_j I_j - \mu I_j - d_I I_j + m_I(I_i - I_j).\end{aligned}\tag{S24}$$

767 Again, the dynamics in the second patch are equivalent but with swapped i and j .

768

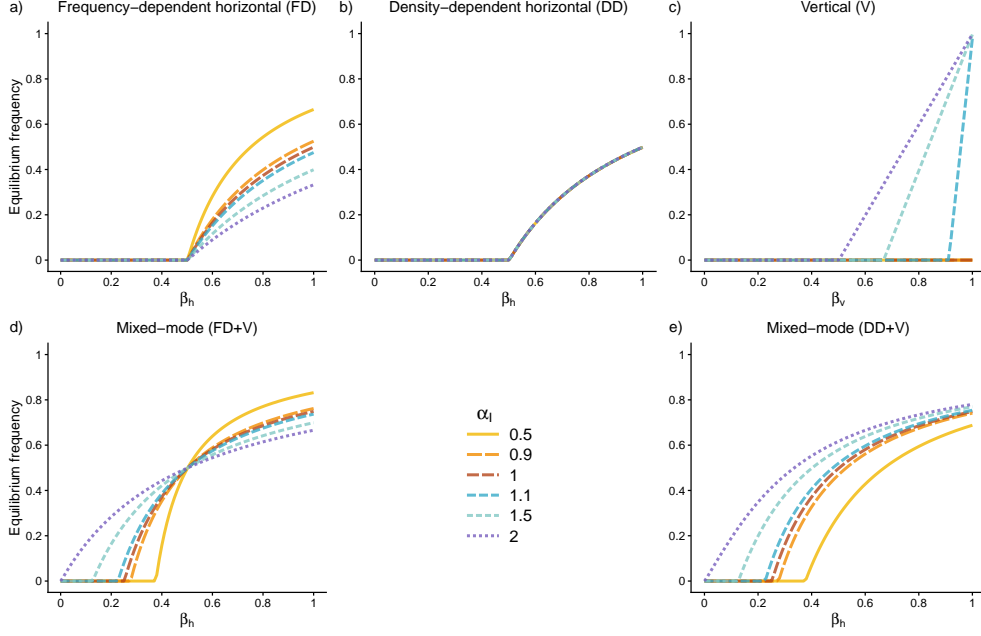


Fig. S7 Change in equilibrium frequency of infected individuals \hat{I} with parasite transmission efficiency β and different per capita birth rate for infected individuals α_I for the different transmission mode scenarios: a) frequency-dependent horizontal transmission, b) density-dependent horizontal transmission, c) vertical transmission, d) mixed-mode transmission with frequency-dependent horizontal and vertical transmission and e) mixed-mode transmission with density-dependent horizontal and vertical transmission. Parameter values: $\alpha_U = 1$, $\mu = 0.002$, $d_U = 0.001$, $d_I = 0.002$, $\theta = 0.001$. The contact rate c was adjusted for the different cases of horizontal transmission. In a) and d) $c = 2$, while in b) and e) $c = 0.002$. In the mixed-mode transmission scenarios vertical transmission efficiency is set to $t_v = 0.5$. Population is initialized with $I = 1$ and $U = 199$.

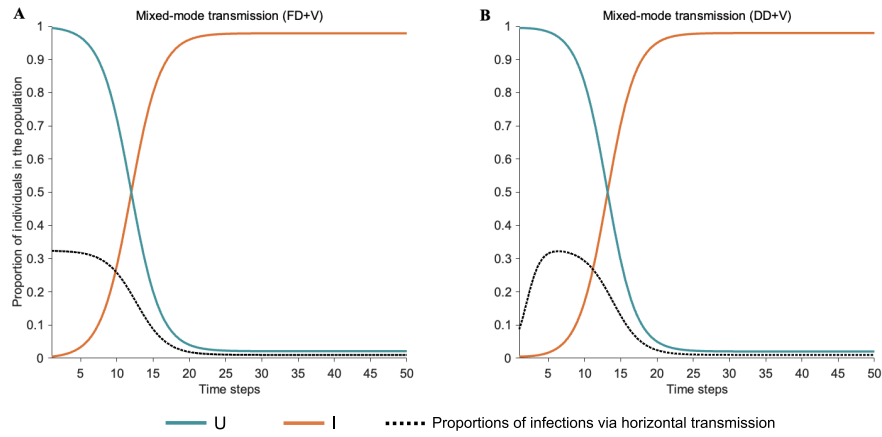


Fig. S8 Proportion of infections via horizontal transmission (dashed line) in the two mixed-mode scenarios compared to the change the proportion of uninfected (blue line) and infected (orange line) individuals in the population over time. Parameter values: $\alpha_U = 1.04$, $\alpha_I = 1.04$, $\mu = 0.0001$, $d_U = 0.001$, $d_I = 0.002$, in A) $c = 0.5$ and in B) $c = 0.0005$, $\beta_h = 0.99$, $\beta_v = 0.99$ and $\theta = 0.001$. Population is initialized with $I = 1$ and $U = 199$.

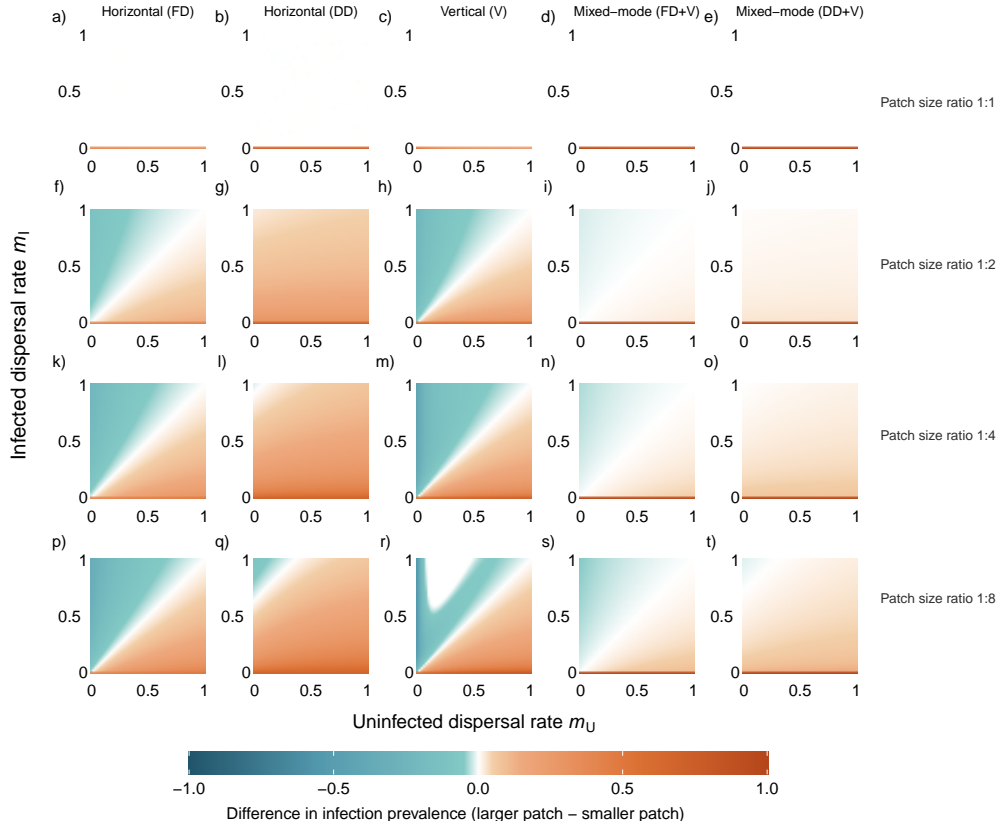


Fig. S9 Infection prevalence difference between two patches for varying dispersal rates, patch size ratios and transmission modes. Heatmap color shows the difference in infection prevalence between two patches (larger patch - smaller patch), where negative values indicate comparatively higher infection prevalence in the smaller patch, while positive values correspond to the larger patch containing higher infection prevalence. The parasite can transmit via frequency-dependent horizontal (a,f,k,p), density-dependent horizontal (b,g,l,q), vertical transmission (c,h,m,r), mixed-mode transmission including frequency-dependent horizontal and vertical transmission (d,i,n,s) or mixed-mode transmission including density-dependent horizontal and vertical transmission (e,j,o,t). In the top row (a-e) patches are the same size, resulting in no difference in infection prevalence, except in the cases, where infected individuals do not disperse $m_I = 0$ and the infection only spreads inside one patch. The difference in size increases with each descending row, with 1:2 ($\theta_{large} = 0.001$, $\theta_{small} = 0.002$), 1:4 ($\theta_{large} = 0.001$, $\theta_{small} = 0.004$) and 1:8 ($\theta_{large} = 0.001$, $\theta_{small} = 0.008$). Other parameters used: $\alpha_U = 1.04$, $\alpha_I = 1.3$, $d_U = 0.001$, $d_I = 0.002$, $\beta_h = 0.9$, $\beta_v = 0.9$, $c_{FD} = 2$, $c_{DD} = 0.0035$ and $\mu = 0.002$.

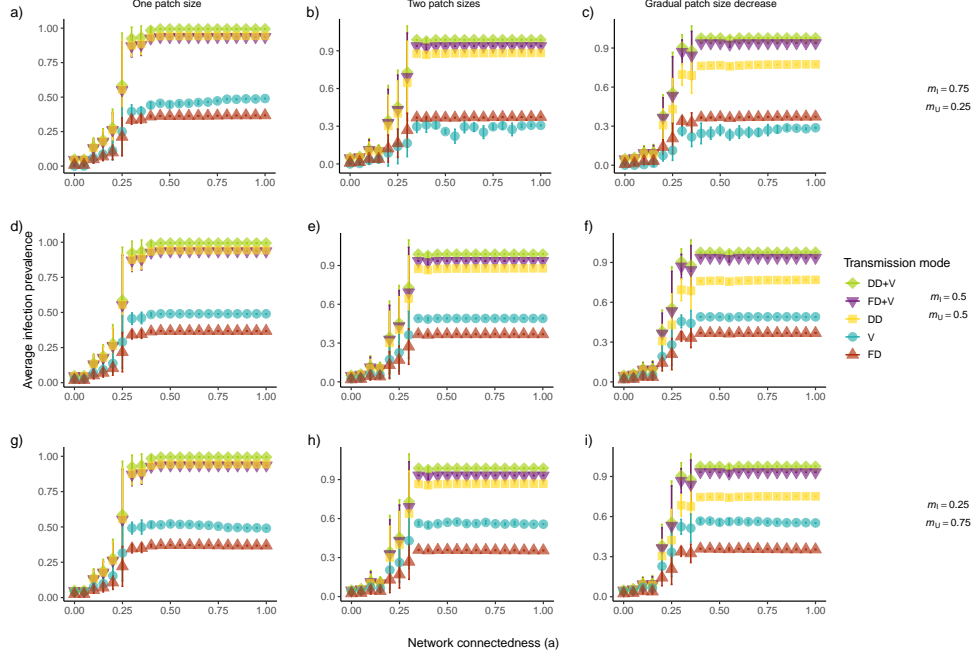


Fig. S10 Impact of transmission mode on global infection prevalence in randomly generated networks. We generate networks of 20 patches, where patch size ratios were either all the same 1:1 with $\theta = 0.001$ (a,d,g), 1:5 (where half of the patches are five times smaller than the other half $\theta_{larger} = 0.001$ and $\theta_{smaller} = 0.005$) (b,e,h) or 1:10 (with $\theta_n = 0.001n$ for $n = 1 : 10$ and two patches of each size) (c,f,i). For each network, we track the global infection prevalence after 1000 timesteps for all parasite transmission modes, while varying connectedness a of the patches. Calculations were repeated for five different randomly generated networks and for three different combination of dispersal propensities: (a-c) $m_U = 0.25$ and $m_I = 75$; (d-f) $m_U = 0.5$ and $m_I = 0.5$; (g-i) $m_U = 0.75$ and $m_I = 25$. All transmission modes are run with to each network. Other parameters: $\alpha_U = 1.04$, $\alpha_I = 1.3$, $d_U = 0.001$, $d_I = 0.002$ $\beta_h = 0.9$, $\beta_v = 0.9$, $c_{FD} = 2$, $c_{DD} = 0.02$, $\mu = 0.002$

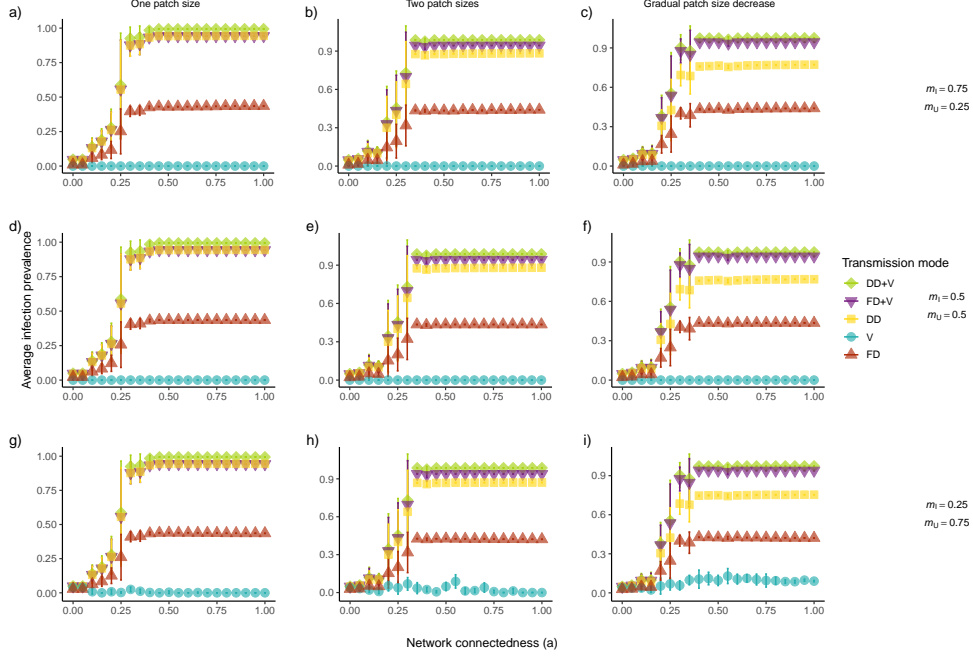


Fig. S11 Impact of transmission mode on global infection prevalence in randomly generated networks. We generate networks of 20 patches, where patch size ratios were either all the same 1:1 with $\theta = 0.001$ (a,d,g), 1:5 (where half of the patches are five times smaller than the other half $\theta_{larger} = 0.001$ and $\theta_{smaller} = 0.005$) (b,e,h) or 1:10 (with $\theta_n = 0.001n$ for $n = 1 : 10$ and two patches of each size) (c,f,i). For each network, we track the global infection prevalence after 1000 timesteps for all parasite transmission modes, while varying connectedness a of the patches. Calculations were repeated for five different randomly generated networks and for three different combination of dispersal propensities: (a-c) $m_U = 0.25$ and $m_I = 75$; (d-f) $m_U = 0.5$ and $m_I = 0.5$; (g-i) $m_U = 0.75$ and $m_I = 25$. All transmission modes are run with to each network. Other parameters: $\alpha_U = 1.04$, $\alpha_I = 0.98$, $d_U = 0.001$, $d_I = 0.002$ $\beta_h = 0.9$, $\beta_v = 0.9$, $c_{FD} = 2$, $c_{DD} = 0.02$, $\mu = 0.002$

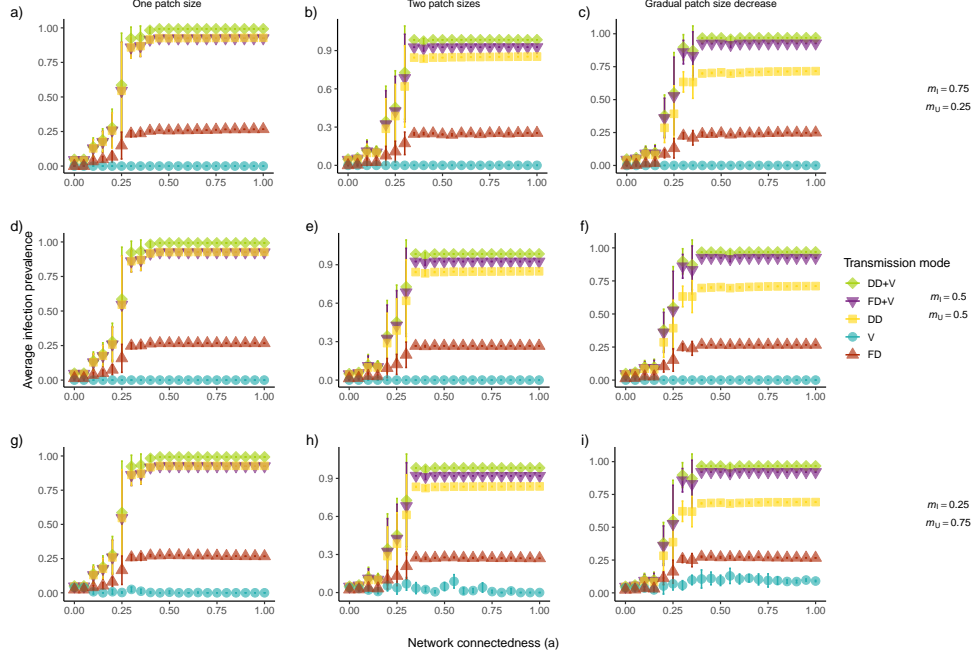


Fig. S12 Impact of transmission mode on global infection prevalence in randomly generated networks. We generate networks of 20 patches, where patch size ratios were either all the same 1:1 with $\theta = 0.001$ (a,d,g), 1:5 (where half of the patches are five times smaller than the other half $\theta_{larger} = 0.001$ and $\theta_{smaller} = 0.005$) (b,e,h) or 1:10 (with $\theta_n = 0.001n$ for $n = 1 : 10$ and two patches of each size) (c,f,i). For each network, we track the global infection prevalence after 1000 timesteps for all parasite transmission modes, while varying connectedness a of the patches. Calculations were repeated for five different randomly generated networks and for three different combination of dispersal propensities: (a-c) $m_U = 0.25$ and $m_I = 0.75$; (d-f) $m_U = 0.5$ and $m_I = 0.5$; (g-i) $m_U = 0.75$ and $m_I = 0.25$. All transmission modes are run with to each network. Other parameters: $\alpha_U = 1.04$, $\alpha_I = 0.98$, $d_U = 0.001$, $d_I = 0.002$ $\beta_h = 0.7$, $\beta_v = 0.9$, $c_{FD} = 2$, $c_{DD} = 0.02$, $\mu = 0.002$

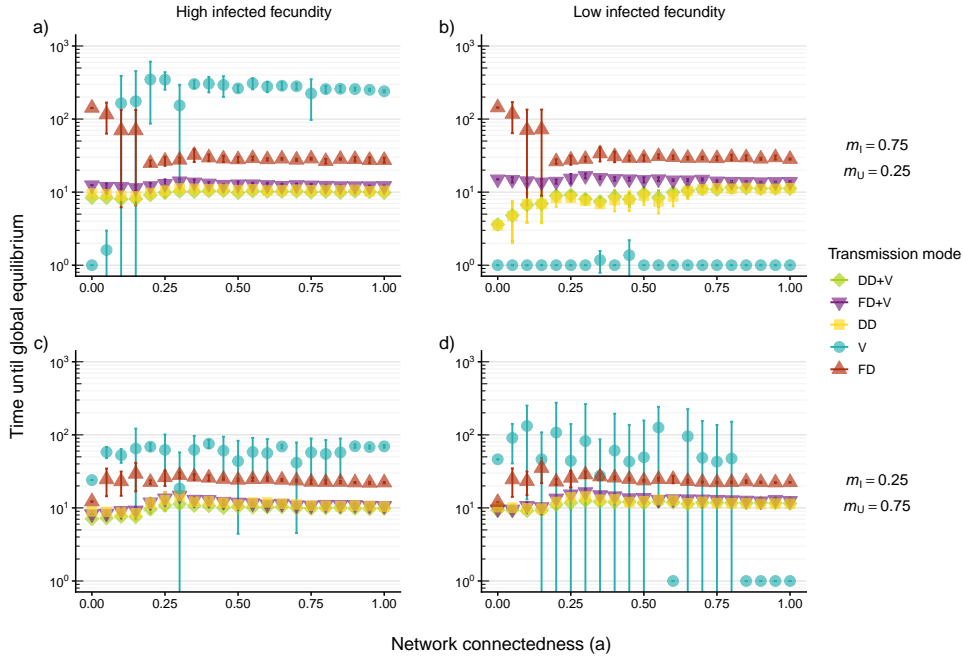


Fig. S13 Impact of transmission mode on time until equilibrium in randomly generated networks. We generate networks of 20 patches, where patch size ratios were either all the same 1:1 with $\theta = 0.001$ (a,d,g), 1:5 (where half of the patches are five times smaller than the other half $\theta_{larger} = 0.001$ and $\theta_{smaller} = 0.005$) (b,e,h) or 1:10 (with $\theta_n = 0.001n$ for $n = 1 : 10$ and two patches of each size) (c,f,i). For each network, we track the global infection prevalence after 1000 timesteps for all parasite transmission modes, while varying connectedness a of the patches. We record the time to equilibrium frequency, defined as the time point at which changes in global infection frequency fall below a threshold of 10^{-17} . Calculations were repeated for five different randomly generated networks and for two different combination of dispersal propensities: (a-b) $m_I = 75$ and $m_U = 0.25$; (g-i) $m_I = 25$ and $m_U = 0.75$. All transmission modes are run with to each network. Other parameters: $\alpha_U = 1.04$, $\alpha_I = 1.3$, $d_U = 0.001$, $d_I = 0.002$ $\beta_h = 0.9$, $\beta_v = 0.9$, $c_{FD} = 2$, $c_{DD} = 0.02$, $\mu = 0.002$